NEW QUANTUM OSCILLATIONS IN MAGNETO TRANSPORT OF A HIGH-MOBILITY TWO-DIMENSIONAL ELECTRON SYSTEM

by

Changli Yang

A dissertation submitted to the faculty of
The University of Utah
in partial fulfillment of the requirements for the degree of

Doctor of Philosophy

Department of Physics

The University of Utah

August 2004

THE UNIVERSITY OF UTAH GRADUATE SCHOOL

SUPERVISORY COMMITTEE APPROVAL

of a dissertation submitted by

Changli Yang

This dissertation has been read by each member of the following supervisory committee and by majority vote has been found to be satisfactory.

_____   _____

                                            Chair: Rui-Rui Du

_____   _____

                                                        Alexei L. Efros

_____   _____

                                                        Feng Liu

_____   _____

                                                        Brian T. Saam

_____   _____

                                                        John M. Worlock

THE UNIVERSITY OF UTAH GRADUATE SCHOOL

FINAL READING APPROVAL

To the Graduate Council of the University of Utah:

I have read the dissertation of _____ Changli Yang _____ in its final form
and have found that (1) its format, citations, and bibliographic style are consistent and
acceptable; (2) its illustrative materials including figures, tables, and charts are in place;
and (3) the final manuscript is satisfactory to the Supervisory Committee and is ready
for submission to The Graduate School.

_____   _____
Date   Rui-Rui Du
               Chair: Supervisory Committee

Approved for the Major Department

_____
Pierre Sokolsky
Chair

Approved for the Graduate Council

_____
David S. Chapman
Dean of The Graduate School

ABSTRACT

Quantum transport in two-dimensional electron systems (2DES) has been one of the major topics in condensed matter physics for many years. Although extensive studies have been performed in the regime of the quantum Hall effect (QHE) where a high magnetic field (typical $B \sim 10$ T) is required, much less attention has been paid to the lower magnetic field regime where the Landau quantization of the 2DES is important but the QHE are absent (typical $B \lesssim 0.5$ T). The 2D transport at the lower B regime was thought to be well understood and no surprise was expected. Contrary to this belief, three new classes of quantum oscillations have been discovered recently by our group (Quantum transport group of the University of Utah, led by Prof. RuiRui Du) in high-mobility 2DES at low magnetic fields.

These new quantum oscillations are 1) the magneto-acoustic-phonon resonance (MAPR) involving *acoustic* phonons (in contrast with the well-known magneto-phonon resonance involving *optical* phonons), 2) the magneto-Zener-tunneling resonance (MZTR), induced by a relatively large dc current, and 3) the microwave-induced photo-conductivity resonance (MIPCR). In ultra-high-mobility samples, the minima of the MIPCR oscillations further develop into the so-called "zero resistance state" (ZRS). All these phenomena are manifested in magnetoresistance by periodic (in $1/B$) oscillations. It is now clear that an important selection rule in 2D transport, namely $q = 2k_F$ in momentum space or $\Delta Y = 2R_c$ in real space, is underlying the MAPR and the MZTR, where q is the electron momentum transferred to a scatterer, k_F is the Fermi wavevector of the 2DES, ΔY is the guiding center shift of a scattered electron, and R_c is the cyclotron radius. This selection rule is not directly related to a conservation law but due to the very sharp cutoff at $\Delta Y = 2R_c$ for the overlap integral between displaced Landau orbits in the vicinity of the Fermi level. On the other hand, the origin of the

MIPCR oscillations and the mechanism leading to ZRS remain open issues and have stimulated considerable current interest in the research community.

In this thesis, all of these newly discovered magneto resonances are discussed, and experimental work participated by the author are presented in detail in the text. Specifically, this thesis describes the following contributions: 1) detailed temperature dependence measurements for the MAPR, whose results strongly suggest the involvement of two branches of acoustic interface phonons, in agreement with the theoretical calculations; 2) original observation and explanation of the MZTR; 3) observation of conductance oscillations and the corresponding "zero conductance state" (ZCS) in samples with Corbino geometry, which indicate the validity of the standard tensor relation between the dc conductivity and resistivity for the ac-driven MIPCR and ZRS.

At the end, suggested applications of these new magneto resonances in the study of composite fermions, quasi-particles responsible for the fractional quantum Hall effect, are suggested and discussed in the context of the analogy between a composite fermion and an electron.

To Lihong, and my parents

CONTENTS

LIST OF FIGURES

xi

ACKNOWLEDGMENTS

CHAPTER 1

INTRODUCTION

Quantum transport in two-dimensional electron system (2DES) has been one of the major topics in condensed matter physics for many years. In the recent two decades, although extensive studies have been performed in the quantum Hall effects (QHEs) regime where a high magnetic field (typical $B \sim 10$ T) is required, much less attention has been paid to lower magnetic field regime where the Landau Quantization of the 2DES is important but the QHEs are absent (typical $B \lesssim 0.5$ T). The 2D transport at the lower B regime was thought to be well understood and no surprises were expected. On the contrary, three new classes of quantum magneto oscillations have been discovered recently [1, 2, 3] in high-mobility 2DESs at low magnetic field. These new quantum oscillations are magneto-acoustic-phonon resonance (MAPR), magneto-Zener-tunneling resonance (MZTR), and microwave-induced photo-conductivity resonance (MIPCR). Remarkably, in ultra-high-mobility samples, the minima of MIPCR oscillations further develop into a peculiar "zero resistance state" (ZRS) [4, 5] which is the focus of considerable current interest. These demonstrate that the 2DES remains rich in new physics and worthwhile to carefully study.

In this chapter, a brief discussion will be given to the previously well-known quantum oscillations in 2D magneto transport, as a background for the three newly discovered oscillations. Specifically, the quantization of a 2DES in a perpendicular magnetic field is presented in Sec. 1.1; and general transport properties of a 2DES are discussed in Sec. 1.2. Various magneto oscillations are then discussed: previously well-known oscillations are presented in Sec. 1.3, and the new ones in Sec. 1.4.

1.1 Two-dimensional electron gas and its Landau quantization

Two-dimensional electron systems(2DESs) are mostly realized in semiconductors, typical structures are shown in Fig. 1.1. Due to the confinement potential along the z direction, the direction perpendicular the interface plane (denoted x-y plane), the motion of electrons in z direction is quantized into discrete energy states while the motion in x-y plane is free. These energy levels due to z confinement are called subbands which have energy spacing of the order of 10 meV. At low temperatures (~ 4 K) and sufficient low electron density (typically $n_e \lesssim 5 \times 10^{11}$ cm^{-2}), only the lowest subband is occupied by electrons which means all electrons have same wavefunction related to the z direction; in this case, the electron system is perfectly 2D, with an energy spectrum

$$E_0(k_{//}) = E_0 + \frac{\hbar^2 k_{//}^2}{2m^*}, \tag{1.1}$$

where E_0 is the energy of the lowest subband, $k_{//}$ is a wave vector in the x-y plane, and m^* is the effective mass of the electrons.

If a strong magnetic field, B, is applied perpendicular to the x-y plane, the free motion of a 2D electron in the plane is further quantized into Landau orbits with discrete energy levels, called Landau levels. This Landau quantization of a 2DES has crucial influences on all aspects of the properties of the 2DES, largely due to the drastic change of the density of states.

The treatment of the Landau quantization is well-known textbook knowledge [7]. However, a brief treatment is still worthy to be repeated here, mainly in order to present a basic picture.

Under a perpendicular magnetic field B ($\mathbf{B}||z$), the Schrödinger equation for an electron of the noninteracting 2DES is

$$\frac{1}{2m^*}(-i\hbar\nabla + e\mathbf{A})^2\psi(x,y) = E\psi(x,y), \tag{1.2}$$

where $\mathbf{A}$ is the magnetic vector potential. If we choose Landau gauge for the vector potential
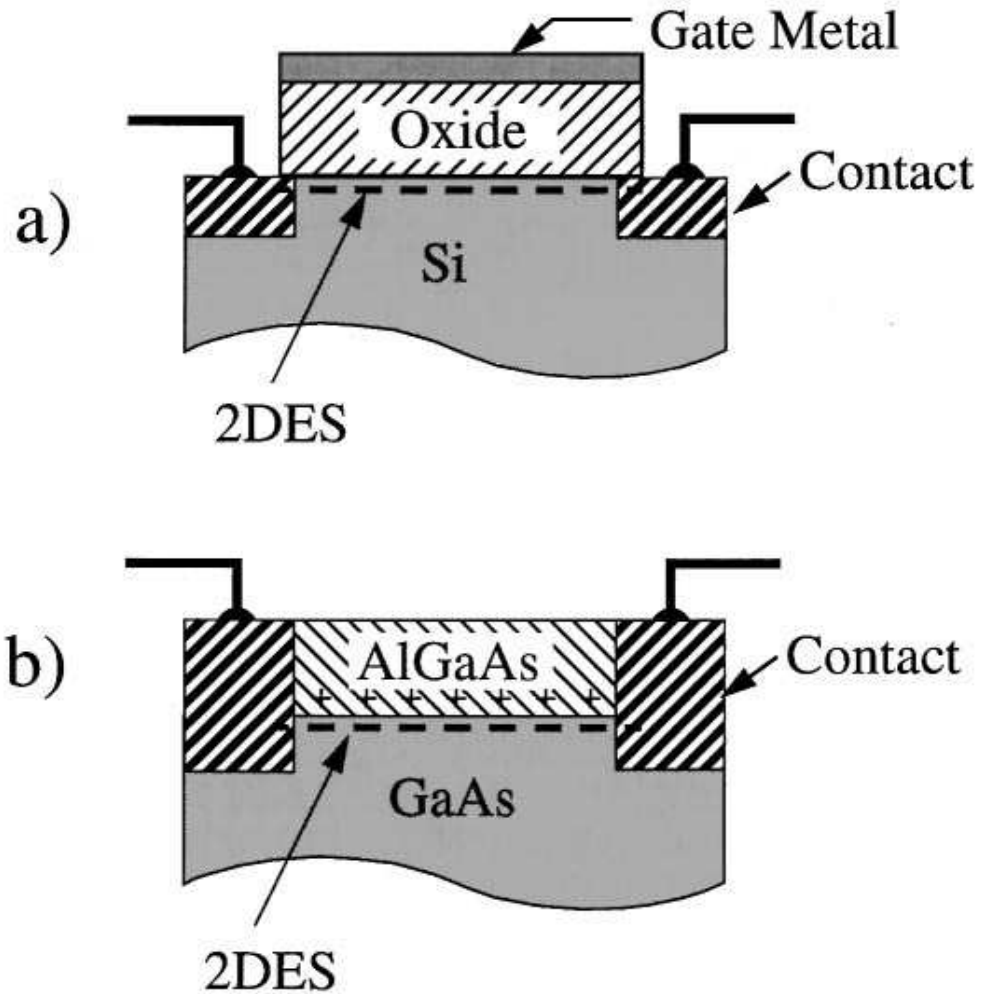
Figure 1.1. Typical structures that host two-dimensional electron system (2DES). (a) A silicon metal-oxidesemiconductor field-effect transistor (MOSFET). The 2DES resides at the interface between silicon and silicon oxide. Electrons are held against the oxide by the electric field from the gate metal; (b) A modulation-doped GaAs/AlGaAs heterojunction. The 2DES resides at the interface between GaAs and AlGaAs. Electrons are held against the AlGaAs by the electric field from the charged silicon dopants (+) in the AlGaAs. [Adapted from Ref. [6].]

$$A_x = -yB, \ A_y = 0, \tag{1.3}$$

then the Hamitonian does not depend on x and the wavefunction can be written as a product of a plane wave in x with an unknown function of y:

$$\psi = e^{ik_x x} u(y). \tag{1.4}$$

Thus the Schrödinger equation becomes

$$\left[-\frac{\hbar^2}{2m^*} \frac{\partial^2}{\partial y^2} + \frac{1}{2} m^* \omega_c^2 (y - l_0^2 k_x)^2 \right] u(y) = E u(x), \tag{1.5}$$

where $\omega_c = eB/m^*$ is the *cyclotron frequency*, and $l_0 = \sqrt{\hbar/m\omega_c} = \sqrt{\hbar/eB}$ is the *magnetic length*. In effect, this is the Schrödinger equation for a one-dimensional harmonic oscillator with shifted center at

$$y = Y = l_0^2 \, k_x. \tag{1.6}$$

Thus we can directly write down the wavefunction and energy for the 2DES under perpendicular magnetic field as:

$$\psi = e^{ik_x x} \phi_n(y - Y), \tag{1.7}$$

$$E_{nY} = (n + \frac{1}{2}) \hbar \omega_c, \tag{1.8}$$

where $\phi_n(y - Y)$ is the solution for the shifted oscillator defined by Eq. (1.5), and $n = 0, 1, 2, 3, \ldots$.

The energy levels in Eq. (1.8) are called *Landau levels*. The degeneracy of each Landau level is given by the number of independent guiding center coordinates Y, hence is determined by the number of allowed k_x according to Eq. (1.6). If the sample has dimensions L_x and L_y, the periodic boundary condition gives $k_x = 2\pi n_x/L_x$ where n_x is limited by

$$0 < |Y| = l_0^2 \, |k_x| = 2\pi l_0^2 n_x/L_x < L_y, \tag{1.9}$$

thus the number of allowed k_x is

$$N_x = max(n_x) = L_x L_y/(2\pi l_0^2). \tag{1.10}$$

It follows that the degeneracy per unit area is

$$n_B = \frac{N_x}{L_x L_y} = \frac{1}{2\pi l_0^2} = \frac{eB}{h} \tag{1.11}$$

which is independent of the material parameters.

In an ideal 2DES, the density of states consists of a series of sharp δ-functions

$$D(E) = n_B \sum_n \delta \left(E - (n + \frac{1}{2})\hbar\omega_c \right). \tag{1.12}$$

However, in real samples, there are always scattering events which broaden the Landau levels and the density of states is given by

$$D(E) = n_B \sum_n \Gamma \left(E - (n + \frac{1}{2})\hbar\omega_c \right), \tag{1.13}$$

where $\Gamma(E)$ is a broadening profile for the Landau levels. It is apparent that the density of states is periodic in the Landau level spacing $\hbar\omega_c$.

For a 2DES with an electron density n_e, the number of occupied Landau levels is given by the *filling factor*

$$\nu = \frac{n_e}{n_B} = \frac{n_e h}{eB}. \tag{1.14}$$

If the magnetic field is swept for a given n_e, the filling factor will continuously change, which is equivalent to a continuous motion of the Fermi level across the Landau levels. From Eq. 1.13, it is clear that this results in an oscillatory density of states (periodic in 1/B) at the Fermi level. The oscillatory density of states (periodic in 1/B) at the Fermi level is reflected in a number of properties of the 2DES, for example, in the magnetic susceptibility and magnetoresistance.

1.2 Magnetoresistance of two-dimensional electron systems

In general, the current density and electric field in a 2DES are related by

$$\mathbf{J} = \sigma \mathbf{E}, \tag{1.15}$$

where the σ is the *conductivity tensor*

$$\sigma = \begin{pmatrix} \sigma_{xx} & \sigma_{xy} \\ -\sigma_{xy} & \sigma_{yy} \end{pmatrix}. \tag{1.16}$$

The *resistivity tensor* is the reciprocal of the conductivity, and it is given by

$$\rho = \frac{1}{\sigma_{xx}\sigma_{yy} + \sigma_{xy}^2} \begin{pmatrix} \sigma_{xx} & -\sigma_{xy} \\ \sigma_{xy} & \sigma_{yy} \end{pmatrix}. \tag{1.17}$$

1.2.1 Semiclassical transport

The 2D transport in a weak magnetic field of a 2DES can be semiclassically treated using the Boltzmann transport equation, without invoking the Landau quantization.

For a homogeneous electron gas under electric field $\mathbf{E}$ and magnetic field $\mathbf{B}$, within the *relaxation time approximation* the Boltzmann transport equation gives

$$-e(\mathbf{E} + \mathbf{v} \times \mathbf{B})\frac{1}{\hbar}\nabla_k f = -\frac{f - f_0}{\tau}, \tag{1.18}$$

where f and f_0 are the distribution functions with and without the external fields, τ is the relaxation time, and

$$\mathbf{v} = \hbar\nabla_k\epsilon(k) \tag{1.19}$$

is the drift velocity. By iteration of Eq. 1.18 to keep the first order of $\mathbf{E}$ and second order of $\mathbf{B}$, it can be shown that

$$f - f_0 = e\tau\frac{\partial f_0}{\partial \epsilon}\mathbf{v}\cdot[\mathbf{E} - \mathbf{E} \times \frac{e\tau}{m^*}\mathbf{B} + (\mathbf{E} \times \frac{e\tau}{m^*}\mathbf{B}) \times \frac{e\tau}{m^*}\mathbf{B}], \tag{1.20}$$

where

$$\frac{\partial f_0}{\partial \epsilon} \approx -\delta(\epsilon - E_F) \tag{1.21}$$

for degenerate electron gas with Fermi level E_F.

The current density is given by

$$\mathbf{J} = \frac{1}{2\pi^2}\int e\mathbf{v}f\, d^2\mathbf{k}. \tag{1.22}$$

Substitution Eq. 1.20 and 1.21 into 1.22, after some manipulations, it follows that

$$\mathbf{J} = \sigma_0[\mathbf{E} - \mu\mathbf{E} \times \mathbf{B} + \mu^2(\mathbf{E} \times \mathbf{B}) \times \mathbf{B}], \tag{1.23}$$

with

$$\sigma_0 = \frac{n_e e^2 \tau}{m^*}, \ \mu = \frac{e\tau}{m^*}. \tag{1.24}$$

Utilizing the fact that $\mathbf{E}$ is in the 2D plane, and $\mathbf{B}$ is perpendicular to the plane, equation 1.23 gives the 2D conductivity

$$\sigma = \sigma_0 \begin{pmatrix} 1 - (\mu B)^2 & -\mu B \\ \mu B & 1 - (\mu B)^2 \end{pmatrix}. \tag{1.25}$$

Thus the resistivity (only keep to the second order of μB) is

$$\rho = \begin{pmatrix} 1/\sigma_0 & B/n_e e \\ -B/n_e e & 1/\sigma_0 \end{pmatrix}. \tag{1.26}$$

It is easy to see that the magnetic field makes no correction to the diagonal resistance, and it only contributes to the Hall effect with an essentially classic Hall resistivity $\rho_{xy} = B/n_e e$.

These results are valid at weak magnetic fields such that $\mu B = \omega_c \tau \ll 1$ (see distribution function of Eq. 1.20: the expansion is only valid at small B otherwise it is incomplete). Also note that this condition means the Landau levels are far from being resolved thus are justified to be ignored. Other key assumptions made are a perfect parabolic energy dispersion and strong degeneracy with a well-defined Fermi surface, which are generally satisfied for typical high mobility 2DES located in GaAs/AlGaAs interfaces at low temperatures.

1.2.2 Quantum transport

In a strong magnetic field such that $\mu B = \omega_c \tau \gg 1$, the Landau levels are well resolved. Such energy quantization by the magnetic field drastically modifies the energy spectrum and the density of states. Although a Fermi level can still be well defined, there is no Fermi surface in the momentum space. In this situation, the magnetic field can no longer be taken as a perturbation but has to be incorporated into the system at the starting point. The electrical transport in this regime is thus called *quantum transport* since the Landau quantization plays a central role and quantum mechanical treatments are essential.

To relate a current density to an electric field, let us consider a 2DES under a perpendicular magnetic field B and an electric field E_y in the plane along the y

direction. The electric field introduces a potential, eE_yy, to the Hamiltonian. In Sec. 1.1, the solution with $E_y = 0$ is already given, so following the same procedures, the solution for $E_y \leq 0$ is easy to get:

$$\psi_{nY} = e^{ik_x x}\phi_n(y - Y), \tag{1.27}$$

$$E_{nY} = (n + \frac{1}{2})\hbar\omega_c + eE_yY + \frac{1}{2}m^*v_d^2, \tag{1.28}$$

with

$$Y = l_0^2\, k_x - \frac{v_d}{\omega_c}, \ \ v_d = \frac{E_y}{B}. \tag{1.29}$$

It is found that the E_y has only two effects to the solution: 1) shifted the guiding centers of the harmonic oscillators (see Eq. 1.29); 2) spatially tilted the Landau levels hence lifted the degeneracy within each Landau level (see Eq. 1.28).

It is easy to evaluate the velocities v_x and v_y:

$$v_x = \ <nY| -i\hbar\frac{\partial}{\partial x} - eyB|nY> = v_d, \tag{1.30}$$

$$v_y = \ <nY| -i\hbar\frac{\partial}{\partial y}|nY> = 0. \tag{1.31}$$

Hence the current densities are obtained:

$$J_x = \ n_e(-e)v_x = -n_eev_d = -\frac{n_ee}{B}E_y, \tag{1.32}$$

$$J_y = \ n(-e)v_x = 0. \tag{1.33}$$

This gives the conductivity tensor

$$\sigma = \begin{pmatrix} 0 & -n_ee/B \\ n_ee/B & 0 \end{pmatrix}. \tag{1.34}$$

Now we can see that for an ideal 2DES under strong magnetic field, the diagonal conductivity is *zero* and the off-diagonal conductivity is the Hall conductivity with the exact classic value. In this case the current is purely a Hall current which is orthogonal to the electric field, so there is no dissipation in the system.

In real systems, scatterers always present. The scattering potential, V, can be perturbatively treated through quantum mechanical approaches, such as by expanding the density operator with respect to V [8, 9, 10]. It can be shown [9]

that to second order of V, the Hall conductivity does not change. However the diagonal conductivity is nonzero due to scattering. In a strong magnetic field, a non-vanishing diagonal conductivity is entirely due to the migration of guiding centers caused by scattering [11], thus a Titeica type formula can be given for the migration current [11, 12]

$$J_y = \frac{e}{L_x L_y} \sum_{\mu\mu'} W_{\mu\mu'}(Y' - Y) f_\mu (1 - f_{\mu'}), \tag{1.35}$$

where $\mu = (NY)$, $\mu' = (N'Y')$ label the initial state and final state, $W_{\mu\mu'}$ is the transition rate in the Born approximation [13], and $f_\mu = 1/(e^{(E_\mu - E_F)/k_B T} - 1)$ is the Fermi distribution of the electrons. The diagonal conductivity can then be calculated through

$$\sigma_{xx} = \sigma_{yy} = \frac{J_y}{E_y} = \frac{1}{E_y} \frac{e}{L_x L_y} \sum_{\mu\mu'} W_{\mu\mu'}(Y' - Y) f_\mu (1 - f_{\mu'}). \tag{1.36}$$

Eq. 1.36 will be referred to in Chapter 3 to account for the magneto-Zener-tunneling resonance. Although the derivation of Eq. 1.36 appears very straightforward, its validity has been justified by more sophisticated methods [9, 10, 14, 15]. This equation is very important and helps in understanding 2D transport in a strong magnetic field as it expresses well the scattering-induced migrations of guiding centers.

It should be emphasized that, in the quantum transport regime where $\sigma_{xy} \gg \sigma_{xx}, \sigma_{yy}$, the diagonal resistivity ρ_{xx} is *directly* proportional to the conductivity:

$$\rho_{xx} = \frac{\sigma_{yy}}{\sigma_{xx}\sigma_{yy} + \sigma_{xy}^2} \approx \frac{\sigma_{yy}}{\sigma_{xy}^2}. \tag{1.37}$$

This fact is quite contrary to the common thinking at weak or zero magnetic field.

1.3   Magnetoresistance oscillations known before 1997

1.3.1   Shubnikov-de Haas (SdH) oscillations

The SdH oscillations [16] are the primary oscillations observed in high mobility 2DES at low temperatures. An example is shown in Fig. 1.2. The oscillations are controlled by the filling factor $\nu = n_e/eB$, and thus are periodic in $1/B$ with a frequency

$$f = g\frac{h}{e}n_e, \tag{1.38}$$

where $g = 1/2$ if the Zeeman-splitting of the spin levels is not resolved, otherwise $g = 1$.

The origin of the SdH can be understood with the help of Eq. 1.36 as follows. At low temperatures, the transport is typically controlled by scatterers such as impurities and acoustic phonons. In the ohmic regime with a vanishing electric field, the transitions are within the same Landau level at the vicinity of the Fermi level, so the transition rate (hence the diagonal conductivity as well as diagonal resistivity, see Eq. 1.37) is proportional to the square of the density of states at the Fermi level ($D(E_F)$). In the last paragraph of Sec. 1.1, we have indicated that $D(E_F)$ is an oscillatory function controlled by ν, which naturally gives the oscillatory structure of SdH.

The SdH effect requires a degenerate electron gas, thus is pronounced at low temperatures such that $k_B T \ll E_F, \hbar\omega_c$.

In high mobility samples, at low filling factor, the SdH effect develops into the famous quantum Hall effects. This topic will discussed in Chapter 5.

1.3.2   Magneto-optical-phonon resonance (MOPR)

The magnetoresistance can exhibit oscillations due to resonance with optical phonons [17]. The contribution to the magnetoresistance is caused by electron transitions between *different* Landau levels through absorption of optical phonons.
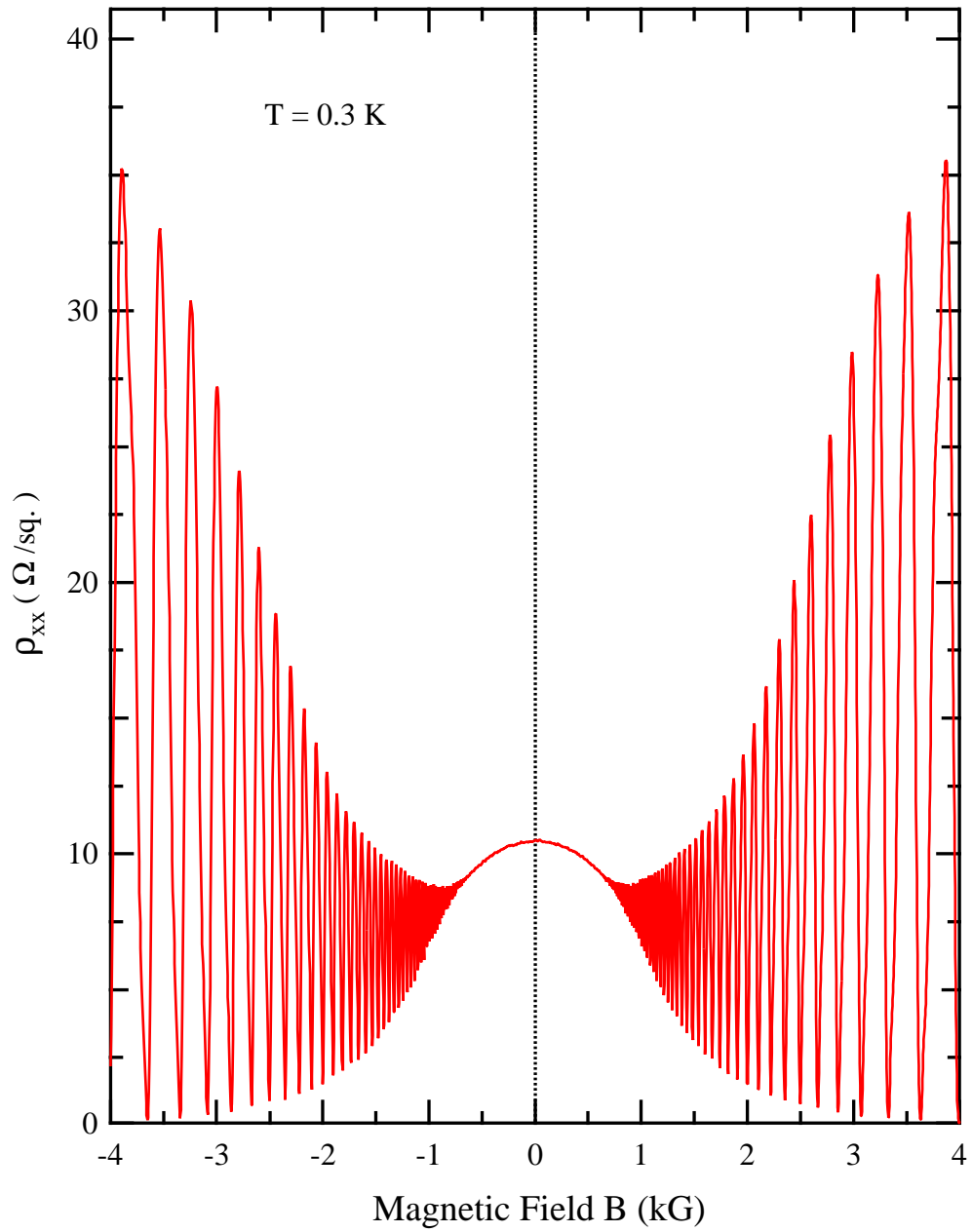
Figure 1.2. SdH oscillations of magnetoresistance observed in a GaAs-Al$_{0.3}$Ga$_{0.7}$As heterostructure with 2D electron density $n_e = 2.1 \times 10^{11}$ cm^{-2} and mobility $\mu \approx 3 \times 10^6$ cm^2/Vs.

Since the dispersion of optical phonons is largely monoenergetic with the energy $\hbar\omega_0$, the energy conservation gives

$$\hbar\omega_0 = j\hbar\omega_c, \; j = 1, \; 2, \; 3, \ldots \; , \tag{1.39}$$

which leads to 1/B oscillations with the frequency

$$f = \frac{m^*\omega_0}{e}, \tag{1.40}$$

independent of the electron density.

The MOPR does not require a degenerate electron gas, and is pronounced at relatively high temperatures (100-180 K) because of the need for optical phonon population.

1.3.3 Geometrical resonance

The geometrical resonance [18, 19] is induced by a periodic spatial potential modulation to the 2DES. This potential modulation broadens every Landau level into an energy band with a oscillatory (in $1/B$) bandwidth, giving rise to an oscillatory current along the direction perpendicular to the potential and also an oscillatory density of states. These lead to the oscillatory conductivity. The oscillations are controlled by the condition

$$2R_c = a(j - 1/4), \; j = 1, \; 2, \; 3, \; \ldots \; , \tag{1.41}$$

where $R_c = l_0^2\sqrt{2\pi n_e}$ is the *cyclotron radius* and a is the period of the modulation potential. The oscillations are periodic in 1/B, with a period proportional to the modulation period.

1.4 Three new classes of quantum oscillations recently discovered

In addition to the well-known magneto oscillations mentioned above, three new classes of oscillations have been discovered by our group in recent years. These new oscillations are briefly summarized in this section and will be detailed in Chapters 2, 3, and 4, respectively.

1.4.1   Magneto-acoustic-phonon resonance (MAPR)

The magneto-phonon resonance involving *acoustic* phonons [1] came as a surprise because the absence of a known selection rule for scattering by acoustic phonons with fixed energy in a sweeping magnetic field. Now it is clear that a momentum transfer rule $q = 2k_F$ generally holds in 2D magneto transport at low magnetic fields [1, 2]. This momentum selection rule is not directly due to the momentum conservation from a single electron transition process, rather it is due to a very sharp cutoff of the overlapping between displaced Landau orbits (namely, $\Delta Y = 2R_c$ in the vicinity of the Fermi level). The condition for the MAPR is then

$$2k_F u = j\omega_c, \ j = 1, \ 2, \ 3, \ \dots \ , \tag{1.42}$$

and the oscillation frequency

$$f = 2k_F u m^*/e. \tag{1.43}$$

1.4.2   Magneto-Zener-tunneling resonance (MZTR)

Usually 2D transport measurements are performed in the ohmic regime where a very small probe current is used (typically, the current density $J < 0.01A/m$). If a relative large current ($J > 0.1A/m$) is passed through a 2DES, the transport gradually becomes non-ohmic. The MZTR is such an non-ohmic effect observed in high mobility 2DESs [2], caused by a relative large Hall field induced by a dc current under a magnetic field. The Hall field makes the Landau levels spatially tilted; hence, the electrons can transit *elastically* between *different* Landau levels with a guide center shift ΔY and give rise to a conductance along the Hall field. In this transport, again, for short-range scattering a selection rule such that $\Delta Y = 2R_c$ exists due to the sharp cutoff of the overlapping between displaced Landau orbits. Then the resonance condition is given by

$$2R_c E_y = j\hbar\omega_c, \ j = 1, \ 2, \ 3, \ \dots \ , \tag{1.44}$$

where $E_y = \frac{J}{n_e e}B$, and frequency is

$$f = \frac{\sqrt{2\pi}m^*}{e^2}\frac{1}{\sqrt{n_e}}J. \tag{1.45}$$

1.4.3   Microwave-induced photo-conductivity resonance (MIPCR)

When it is exposed to a microwave radiation, a high-mobility 2DES exhibits remarkable photoconductivity oscillations [4] which are controlled by the ratio between the microwave frequency and the cyclotron frequency, i.e., $\epsilon = \omega/\omega_c$. In ultra-high-mobility samples, the minima of the oscillation further develop into the so-called "zero resistance states" [4, 5] — and have been shown to be also "zero conductance states" [20]. These experimental findings have stimulated considerable current interest in the research community.

CHAPTER 2

MAGNETO RESONANCE CAUSED BY LEAKY INTERFACE ACOUSTIC PHONONS

The magnetophonon resonance effect (MPR) in a 2D electron system (2DES) is well known in GaAs-AlGaAs [21, 22, 23, 24, 25] (for a review, see Ref. [17]) and other semiconductor materials. The condition responsible for MPR is $\omega_{ph} = j\omega_c$, were j is an integer, ω_{ph} and $\omega_c = eB/m^*$ are the optical phonon and cyclotron frequencies, respectively, and m^* is the effective mass of the carrier. In transport experiments the MPR manifest as periodic oscillations (in $1/B$) in magnetoresistance, and the period is independent of the electron density. MPR are observed only in a relatively high temperature range (100-180 K) where the optical phonons are populated.

Acoustic modes, because of their dispersion and a lack of known selection rules, have never been considered relevant in MPR. Only recently have the MPR by acoustic-phonons been observed in a high-mobility 2DES in GaAs/Al$_x$Ga$_{1-x}$As heterostructures [1]. The specific modes involved are so-called leaky interface-acoustic phonons (LIAP). Detailed temperature-dependence data [26] revealed two branches of acoustic phonons involved in this MPR, which are consistent with the theoretical calculation for the LIAP phonon modes [27].

In this chapter, Sec. 2.1 is a short review for the *novel* MPR by acoustic-phonons. Sec. 2.2 presents our detailed temperature-dependence data which clearly show the involvement of two branches of acoustic phonons. More experimental data on higher mobility samples are presented in Sec. 2.3.

2.1 Observations of magneto-acoustic-phonon resonance (MAPR)

The magneto-acoustic-phonon resonance (MAPR) discussed in this chapter was discovered experimentally in year 2000 prior to a theoretical explanation; example traces are shown in Fig. 2.1. As usual, the oscillations were found to be periodic in 1/B; however, the density dependence of the oscillation frequency ($f \propto \sqrt{n}_e$) told that the oscillations could not be attributed to any known mechanism. Quantitatively, the condition for the resonance peaks were found to be

$$2k_F u = l\omega_c, \ l = 1, \ 2, \ 3, \ ... \ , \tag{2.1}$$

where $k_F = \sqrt{2\pi n_e}$ is the Fermi wave number of 2DEG at zero B field, and $u \approx 3.0 \times 10^3$ m/s is very close to the sound velocity of GaAs.

Eq. 2.1 strongly suggested a magneto resonance by acoustic phonons, which was partially suported by the fact that the oscillations appear only in a limited temperature range (approximately, $2 < T < 10$ K). In this scenario, Eq. 2.1 is the condition of energy conservation while electrons are scattered by acoustic phonons with momentum $q = 2k_F$. However, there were two difficulties associated with this explanation: (a) An additional momentum selection rule for phonons such that $q = 2k_F$ is needed, and (b) Because of the 2D nature of the electrons, only in-plane momentum can be transferred between electrons and phonons, hence the momentum selection rule should only involve the in-plane wavevector of the phonons. Therefore, Eq. 2.1 implies the phonons involved should have 2D nature because it does not involve q_z [28]. Such 2D phonons were not previously reported in GaAlAs/GaAs heterostructures.

These difficulties within the proposed MPR scenario were successfully resolved by subsequent theoretical studies. Indeed, branches of 2D acoustic phonons were revealed by theoretical calculations [27]. These phonons, called "leaky interface-*acoustic* phonons", are found to be propagating on the GaAlAs/GaAs interface with a complex velocity, $u = u_R + u_I$ where $u_I \ll u_R$. In low magnetic field quantum
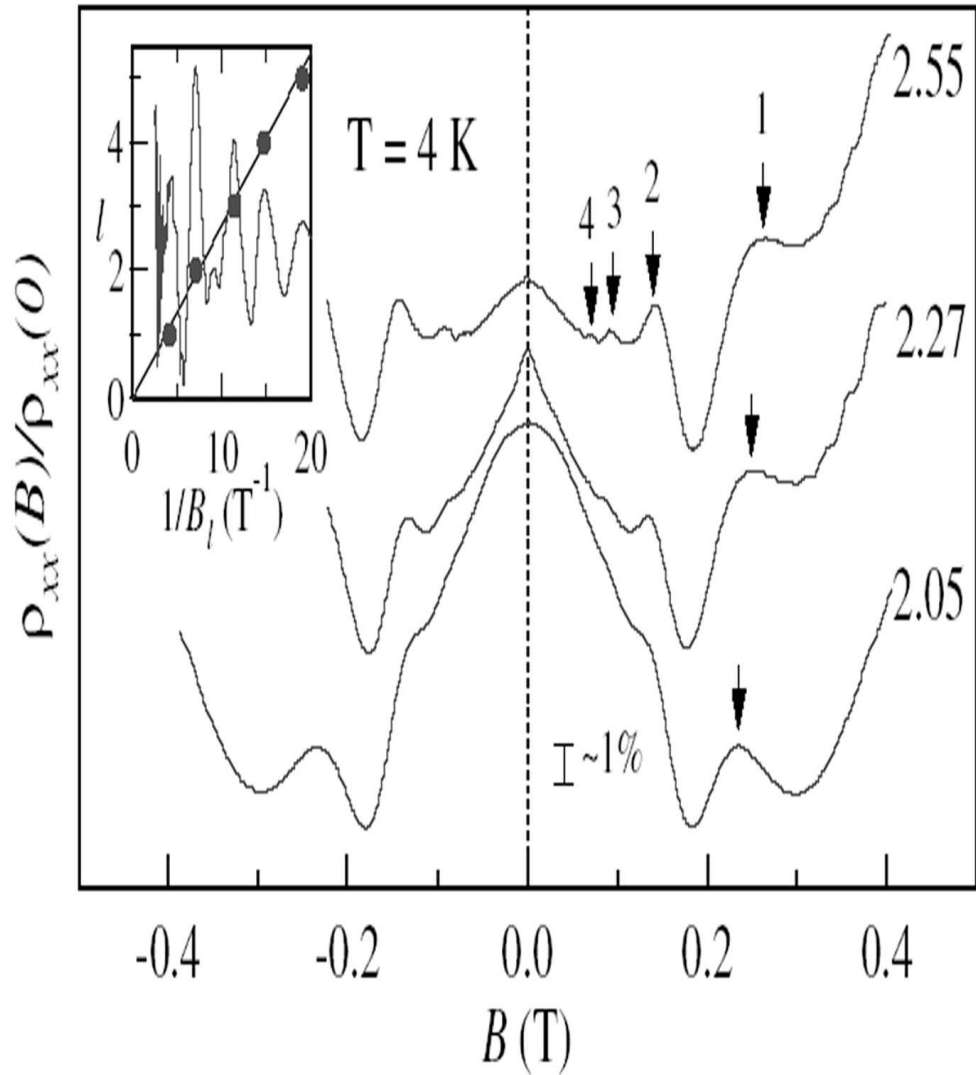
Figure 2.1. Magneto-*acoustic*-phonon resonances observed in a high-mobility GaAS/Al$_{0.3}$Ga$_{0.7}$As heterostructure. Traces (shifted vertically for clarity) are shown for three electron densities n_e of 2.05, 2.27, and 2.55 $\times$ 10^{11} cm^{-2}. Four resonance peaks are observed for $n_e = 2.55 \times 10^{11}$ cm^{-2}, as indicated by arrows. The shift toward higher B with increasing n_e is also indicated by arrows. The inset shows the oscillations (well resolved in $-d^2\rho_{xx}(B)/dB^2$) are periodic in $1/B$. [adapted from Ref. [1].]

transport, the momentum selection rule, $q = 2k_F$, was theoretically derived for the leaky interface phonons [1]. The new magneto oscillations were then well explained as a magneto-phonon resonance involving the leaky interface-*acoustic* phonon modes.

2.2 Evidence for the involvement of two branches of leaky interface acoustic phonons

As discussed above, the novel magneto resonance corresponds to electron transitions between different Landau levels by absorbing a acoustic phonon with momentum $2k_F$. It is easy to see that such MPR is periodic in $1/B$ with a frequency

$$f = 2k_F u m^*/e, \qquad (2.2)$$

hence linear with phonon velocity. In our MPR experiments the phonon velocity can be determined from the oscillation frequency.

In Ref. [1], fast Fourier transformation (FFT) performed on traces at $T \approx$ 4 K has shown that there are two branches of LIAP modes involved in the MPR (with sound velocity $u \approx 2.9$ km/s and $u \approx 4.4$ km/s, respectively). However, more evidence is needed to support this observation. In this section, more detailed measurements on the temperature dependence of the oscillation amplitudes are presented, which confirms the involvement of two branches of LIAP modes. At $T \approx 4$ K the oscillation features result predominately from the resonance with a LIAP mode of velocity $u \approx 3.0$ km/s. With increasing temperature, however, the features are gradually dominated by a higher velocity mode with $u \approx 4.6$ km/s. These results are in qualitative agreement with the calculations [27] for the GaAs/Al$_x$Ga$_{1-x}$As interface.

2.2.1   Samples and methods

Our samples are lithographically defined Hall bars cleaved from GaAs/Al$_{0.3}$Ga$_{0.7}$As heterostructures of a high-mobility $\mu \approx 3 \times 10^6$ cm^2/Vs.

The data presented here are from a Hall bar sample of width 50 μm, although data with comparable quality were obtained from a variety of samples. The electron density n_e can be tuned by shining a red LED and by applying voltage to a NiCr front gate. The magnetoresistance traces $\rho_{xx}(B)$ at various temperatures (from 1.5 to 10 K) were measured using a variable-temperature ^{4}He cryostat and a superconducting magnet, employing a standard low-frequency lock-in technique. The frequency of the MPR were then obtained from FFT performed on $-d^2\rho_{xx}(B)/dB^2$ with respect to $1/B$.

2.2.2 Experimental results

In Fig. 2.2 we show the low-field magnetoresistivity $\rho_{xx}(B)$ measured at $T = 3.9$ K, for electron density (in units of 10^{11} cm^{-2} throughout the text) $n_e = 2.12$, 2.54, and 3.45, respectively. A major feature of the MPR is the oscillatory structure in the field range $B < 5$ kG. The inset of Fig. 2.2 shows the corresponding FFT power spectra of the magnetoresistance traces. In the lower frequency range (2 $\sim$ 5 kG), two peaks (marked by A and B) appear corresponding to a sound velocity $u_A \approx 3.0$ km/s and $u_B \approx 4.6$ km/s, respectively. The high-frequency peaks are due to SdH oscillation. Notice that the frequency of SdH effect is linear with n_e, whereas that of the MAPR oscillation is linear with $\sqrt{n_e}$ [1].

The temperature dependence of the FFT amplitudes is consistent with a thermally-excited LIAP resonance model. The magnetoresistance traces at selected temperatures in the range of 1.5 to 10 K are shown in Fig. 2.3. It is apparent that the oscillations are best developed at around $T \sim 4$ K and are damped at both lower and higher T. Qualitatively this can be understood by considering the population of phonons at different temperatures. The dampening at lower T is due to the lack of LIAP phonons carrying momentum $q = 2k_F$, and the dampening at higher T is due to the smearing of Landau levels, by either bulk or interface phonons.

Fig. 2.4 shows the corresponding FFT spectra of the resistivity traces. First, we can see that, with increasing temperature, the amplitudes of the oscillations increase at lower T reaching their maximum at $T \approx 4$ K, and then diminish at a
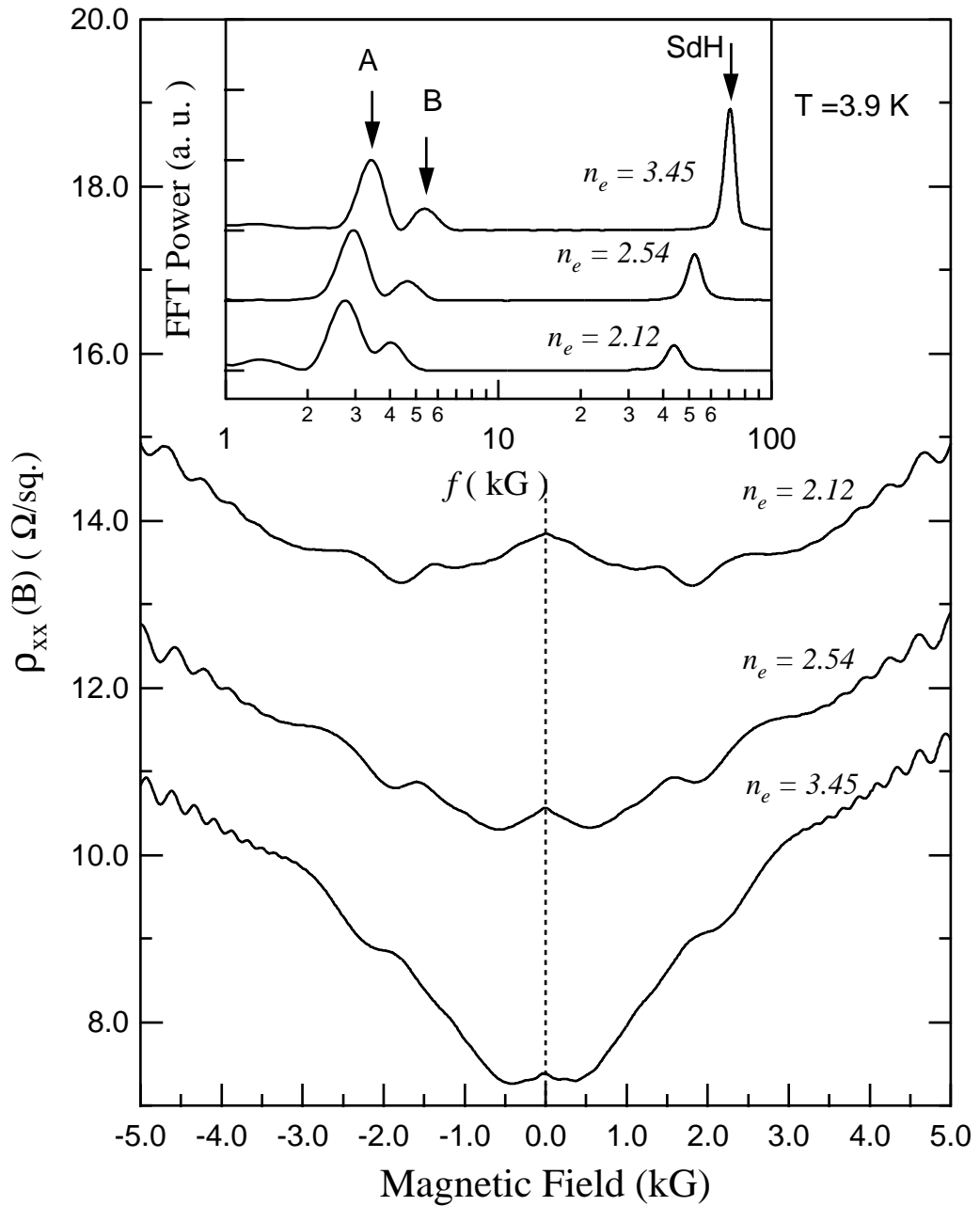
Figure 2.2. Magnetoresistance oscillations arising from the magnetophonon resonance by leaky interface-acoustic modes at $T = 3.9$ K are shown for different densities $n_e = 2.12$, 2.54, and 3.45×10^{11} cm^{-2}. The inset shows the FFT power spectra of the resistivity traces: Peak A and B indicate two branches of phonon modes with velocities $u_A = 3.0$ km/s and $u_B = 4.6$ km/s, respectively; and the SdH peak gives n_e.
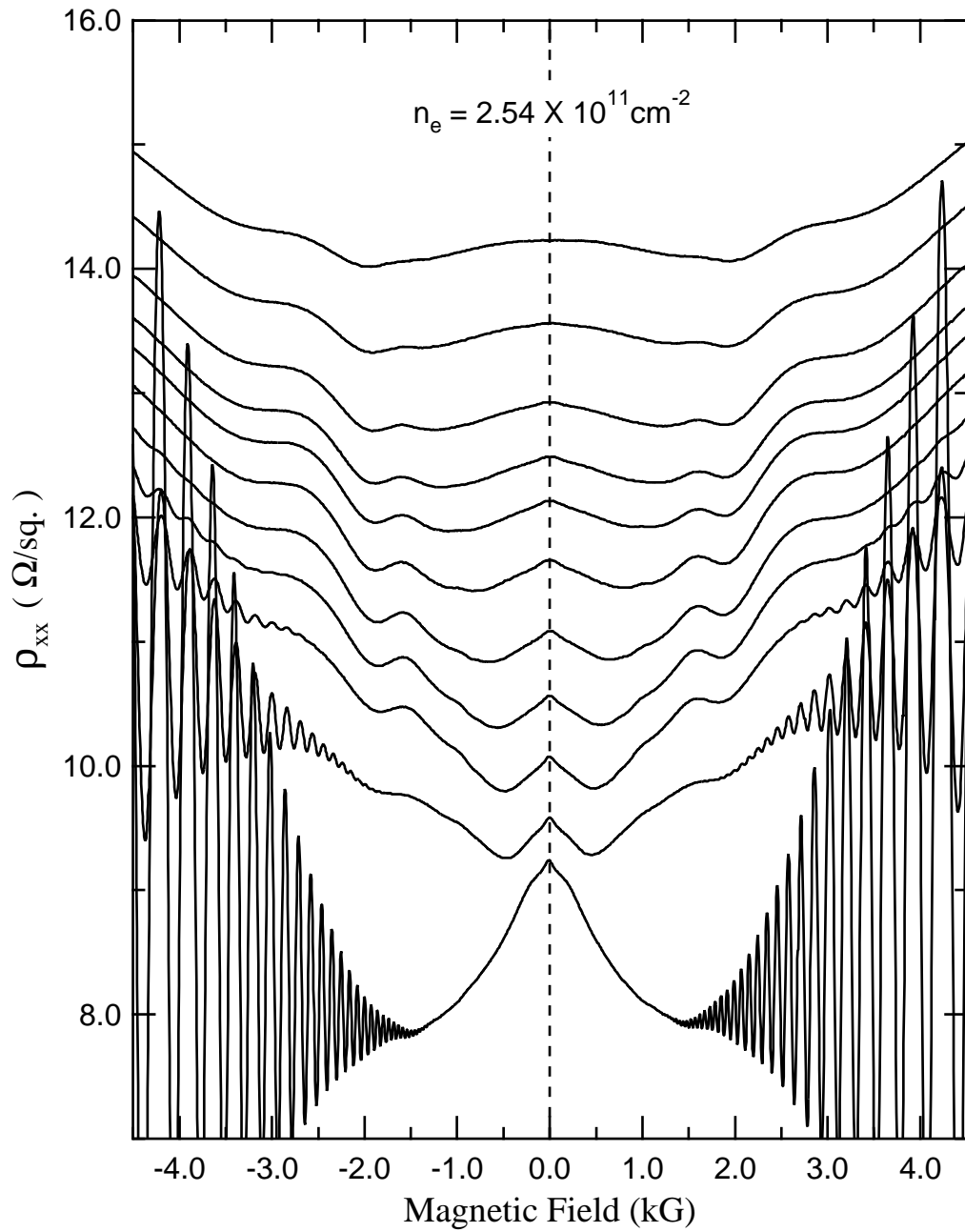
Figure 2.3. Magneto-resistivity traces at selected temperatures (from top: 9.5, 8.5, 7.5, 6.7, 6.2, 5.3, 4.6, 3.9, 3.0, 2.1, 1.5 K) show that the oscillations are best developed at $T \sim 4$ K, and are damped at both lower and higher temperatures.
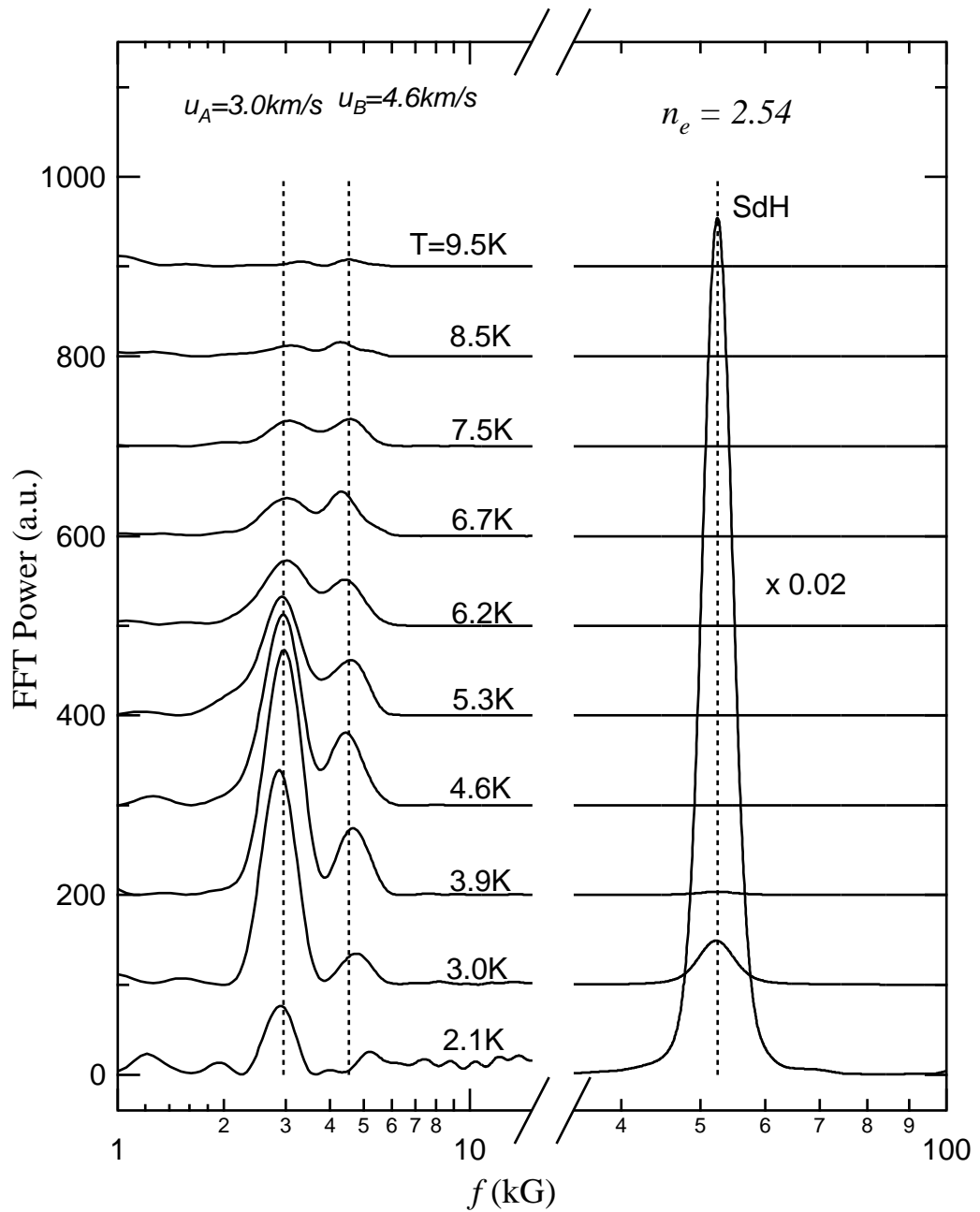
Figure 2.4. The FFT power spectra of the resistivity traces show that at $T < 5$ K the lower velocity phonon mode dominates the resonance, while at $T > 7$ K the higher velocity mode tends to dominate the resonance.

higher T. This result reinforces the observation from Fig. 2.3. Second, we note that the ratio between the amplitude of mode B and that of mode A increases with increasing T. At T below ~ 5 K the lower velocity mode dominates the resonance, while at T above ~ 7 K the features are strongly influenced by the higher velocity mode. This behavior can be qualitatively explained by the Planck distribution of phonon numbers at a given temperature. However, a quantitative analysis of the relative contribution from each mode to the resonance is difficult. In particular, different LIAP modes may interact with electrons with a different strength, thereby complicating the comparison of the amplitude between different modes.

2.2.3 Conclusion

In summary, we have presented a careful temperature dependence measurement for the magnetophonon resonance caused by leaky acoustic-interface modes on $GaAs/Al_xGa_{1-x}As$ interface. The resonance oscillations are best developed at $T \approx 4$ K and are damped at both lower and higher temperatures. FFT analysis clearly shows two branches of phonon modes involved into the resonance. The resonance amplitudes obtained from FFT show that at T below 5 K the lower velocity mode dominates the resonance, and that the oscillation features are strongly influenced by the higher velocity mode with increasing temperatures. The observation can be qualitatively explained via the thermal distribution of the phonon numbers of these two phonon modes.

2.3 MAPR observed on samples with higher mobility

With higher mobility samples, we have observed much stronger MAPR. An example trace is shown in Fig. 2.5. We understand the importance of the mobility as following. The mobility is not only related to the Landau level width but also related to the background resistance. The higher the mobility, the lower the resistance contributed by other scattering mechanism (mainly impurity scattering), thus more prominent the phonon resonance.
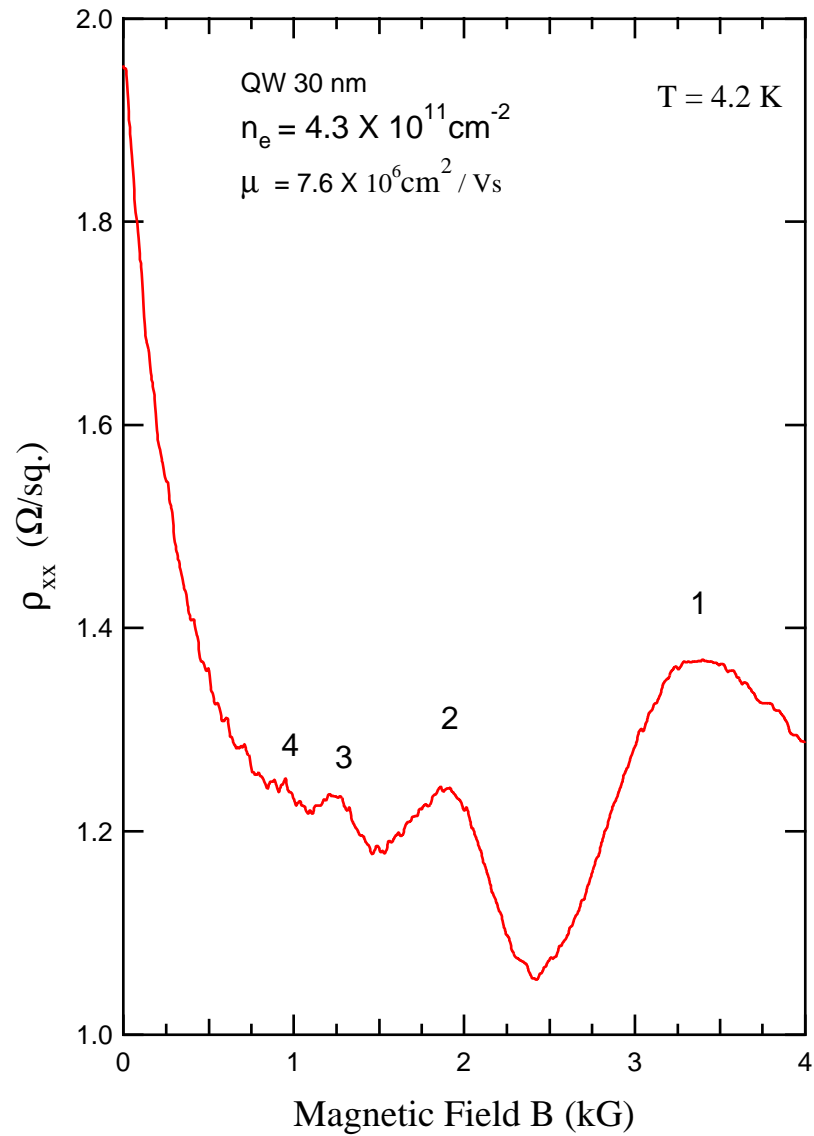
Figure 2.5. MAPR observed on a quantum well (QW) sample with mobility $\mu \approx 8 \times 10^6$ cm^2/Vs. The resonance is much stronger than that from sample with lower mobility $\mu \approx 3 \times 10^6$ cm^2/Vs (see Fig. 2.1).

CHAPTER 3

MAGNETO-ZENER-TUNNELING
RESONANCE: ROLE OF THE
HALL FIELD

In Chapter 2, the magneto-phonon resonance in a high mobility 2DEG is presented. The magneto oscillations are caused by the absorption of leaky interface acoustic phonons originated at the GaAlAs/GaAs interface. Conceptually, a magneto oscillation can also be induced by emission of phonons if the electron is heated up to a temperature significantly higher than that of the lattice, as observed in magneto-optical-phonon resonance [25]. This motivated us to pass a relatively large DC current, intended to heat the electrons, through the samples which showed clear magneto-phonon resonance. Instead of the phonon emission features, surprising new magneto oscillations were discovered following these experiments. The new magneto oscillations are periodic in $1/B$, which is common for quite a few known low field magneto oscillations. However, the oscillation period is found to be directly proportional to the current density J_{dc}. This remarkable characteristic distinguishes this magneto oscillations from any known ones.

The newly discovered oscillations were quickly quantitatively explained by using a simple model based on a selection rule of the electron hopping distance between the spatially tilted Landau levels. Later we came to be aware that a similar mechanism, called Zener tunneling mechanism, had been proposed to account for the breakdown of the integer quantum effect [29]. The Zener tunneling mechanism has not been considered, however, in a low magnetic field regime until our experiments.

3.1   New magneto oscillations induced by a DC current

3.1.1   Samples and measurement setup

Our samples were cleaved from a wafer of a high-mobility GaAs-Al$_{0.3}$Ga$_{0.7}$As heterostructure grown by molecular-beam epitaxy, having an electron density $n_e \approx$ 2×10^{11} cm^{-2} and a mobility $\mu \approx 3 \times 10^6$ cm^2/Vs at a temperature $T = 4.2$ K. Such parameters were obtained after a brief illumination from a light-emitting diode. The distance between the electrons and the Si δ-doping layer is $d_s \approx 70$ nm. Four Hall bar specimens of width $w = 200,\ 100,\ 50,$ and 20 μm were processed by photolithography and wet etching. The 50 μm specimen has a NiCr front gate so that its electron density can be tuned between 1.9 and 4.0×10^{11} cm^{-2}. The experiments were performed in a sorption-pumped ^3H_e cryostat equipped with a superconducting magnet.

In principle, the Zener tunneling effect can be detected in standard magnetoresistance, $R_{xx}(B)$. However, in order to increase the sensitivity, a differential resistance r_{xx} was measured in the following fashion. A constant dc current I_{dc} was passed through the Hall bar, along with a small (100 nA) low frequency ($f = 23$ Hz) modulation current, i_{ac}. The differential magnetoresistance at the given dc bias, $r_{xx} = (\partial V/\partial I)_{I_{dc}} = v_{ac}/i_{ac}$, was then recorded by a lock-in amplifier at the modulation frequency. A schematic circuit for the electrical measurement is shown in the inset of Fig. 3.1.

3.1.2   Observations of new magneto oscillations

Our central finding concerns the strong oscillations in a differential magnetoresistance in the weak magnetic field region, $B < 4$ kG. In Fig. 3.1 we show such features from a 50 μm Hall bar measured at $T = 0.33$ K, for $I_{dc} = 0,\ 10,\ 20,\ 30,\ 40,\ 50$ μA, respectively. For a zero dc bias current, the trace shows well-resolved Shubnikov de-Haas (SdH) oscillations for $B > 0.5$ kG. New oscillations emerge when a finite I_{dc} is applied to the specimen. Up to three
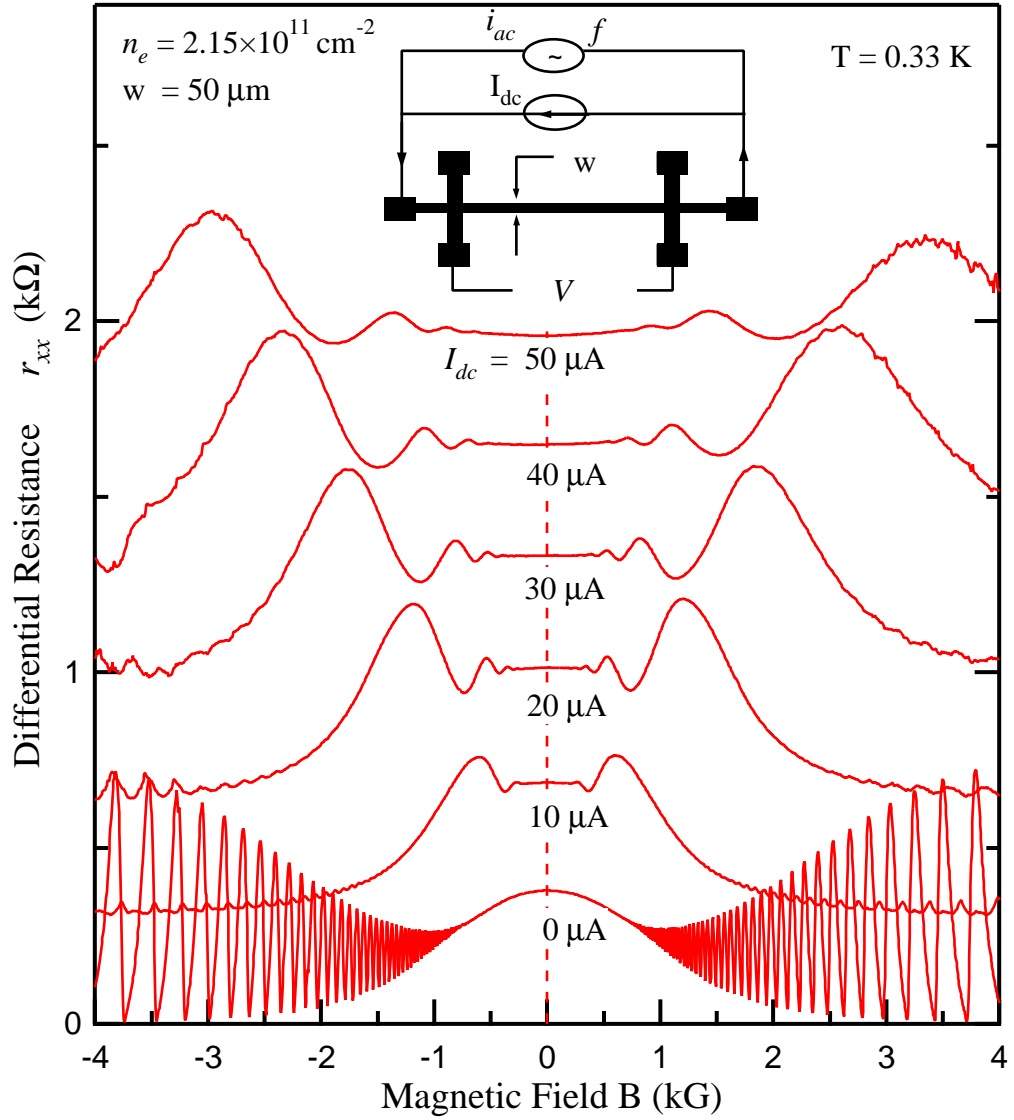
Figure 3.1. The measured differential magnetoresistance traces at various dc current I_{dc} are shown for a 50 μm Hall bar (the traces are shifted vertically for clarity). Up to three orders of oscillations are clearly seen from the traces, and the oscillations are roughly periodic in $1/B$. The inset is a diagram for the electrical measurement.

orders of peaks can be clearly seen from the traces. Furthermore, the peaks shift towards higher B with increasing I_{dc}. The weakening of the SdH effect can be attributed partially to electronic heating by the dc bias. In contrast to the SdH oscillation whose amplitude diminishes quickly at increasing temperatures, the new oscillations persist to a temperature up to $T = 4K$.

It is apparent that the new oscillations, observed here in r_{xx}, are roughly periodic in $1/B$. However, as can be shown, the exact resonance condition for Zener tunneling should correspond to peaks in its derivative, *v. z.*, in $\partial r_{xx}/\partial |B|$ traces [30]. To illustrate this point, we show in Fig. 3.2 the $\partial r_{xx}/\partial |B|$ trace which is obtained by numerical differentiation performed on the $r_{xx}(B)$ trace from a 50 μm sample with a bias $I_{dc} = 30 \ \mu A$. The inset, $1/B_l$ vs. l, confirms that the oscillation in $\partial r_{xx}/\partial |B|$ is strictly periodic in $1/B$.

Remarkably, the oscillation period is tunable by the bias current I_{dc}. In Fig. 3.3 we plot the maximum positions B_l (1, 2, 3), obtained from $\partial r_{xx}/\partial |B|$, against the current density $J_{dc} = I_{dc}/w$, for the four samples. Roughly, all data collapse according to

$$B_l \propto \frac{J_{dc}}{l}. \tag{3.1}$$

3.2 Quantitative explanation by the Zener tunneling mechanism

Such oscillations arise owing to a new scattering channel opened up by a tilted Hall potential. To begin with we consider a 2DEG system under crossed electric and magnetic field, depicted in Fig. 3.4. The electric field is a Hall field along the $-y$ direction, $E_y = v_d B$, induced by a dc current density $J_{dc} = n_e e v_d$, where v_d is the drift velocity of the electrons..

The 2DEG is quantized into a series of Landau levels and has a wave function (see Eq. 1.27)

$$|NY\rangle = \frac{e^{ik_x x}}{\sqrt{L_x}}\phi_N(y - Y), \tag{3.2}$$

where N is the index of Landau levels, and $\phi_N(y-Y)$ is an oscillatory wave function centered at $Y = -l_B^2(k_x - m^* v_d/\hbar)$, with $l_B = \sqrt{\hbar/eB}$ the magnetic length.
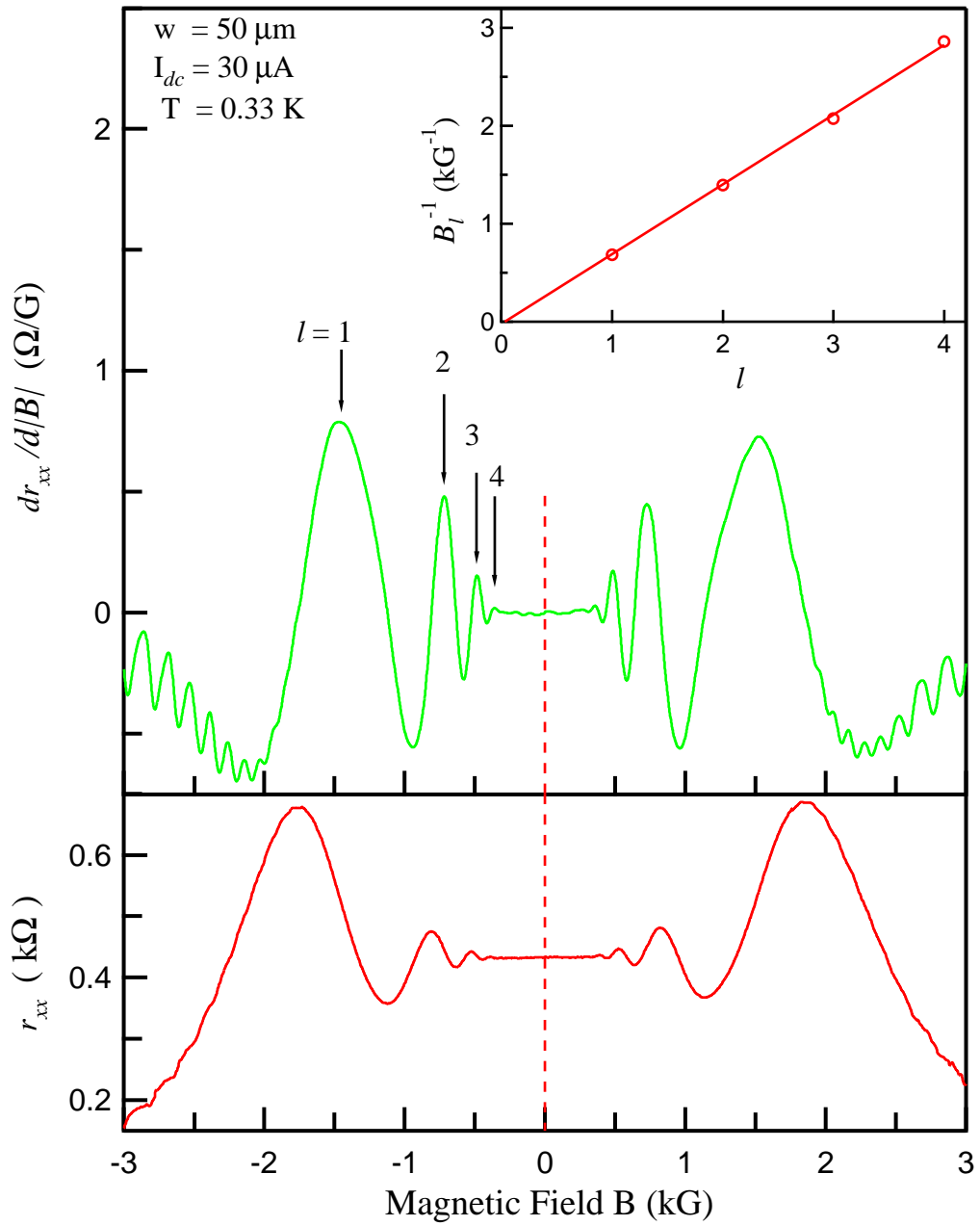
Figure 3.2. The differential magnetoresistance r_{xx} at $I_{dc} = 30 \ \mu A$ for the 50 μm Hall bar is illustrated together with its derivative $\partial r_{xx}/\partial|B|$. The inset shows the precise $1/B$ periodicity extracted from the $\partial r_{xx}/\partial|B|$ trace.
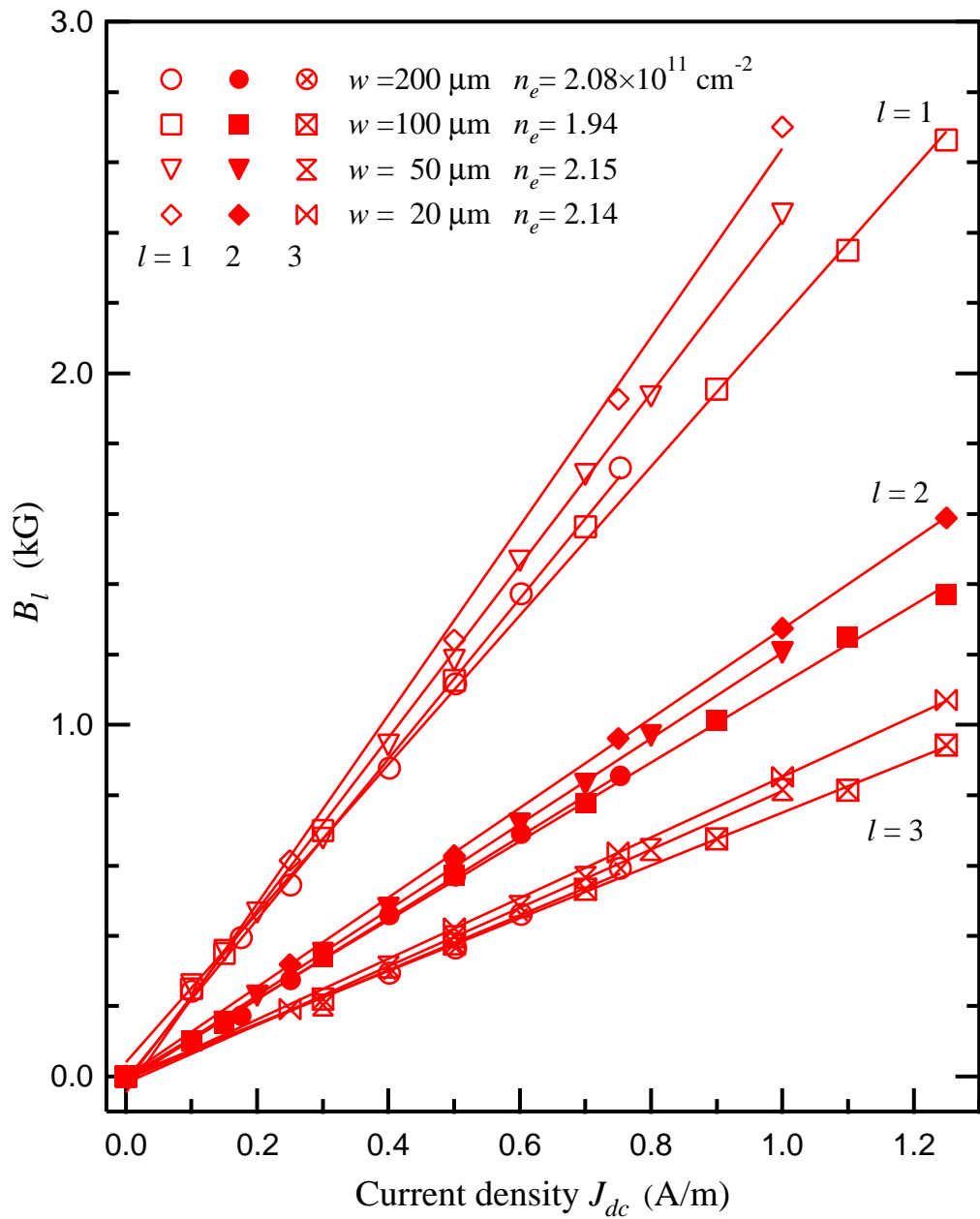
Figure 3.3. The oscillation maxima B_l ($l = 1, 2, 3$) versus current density J_{dc} are shown as a fan diagram for the Hall bars with different width w. A linear fit reveals the relation $B_l \propto J_{dc}/l$, and the slope is nearly the same for all the samples.
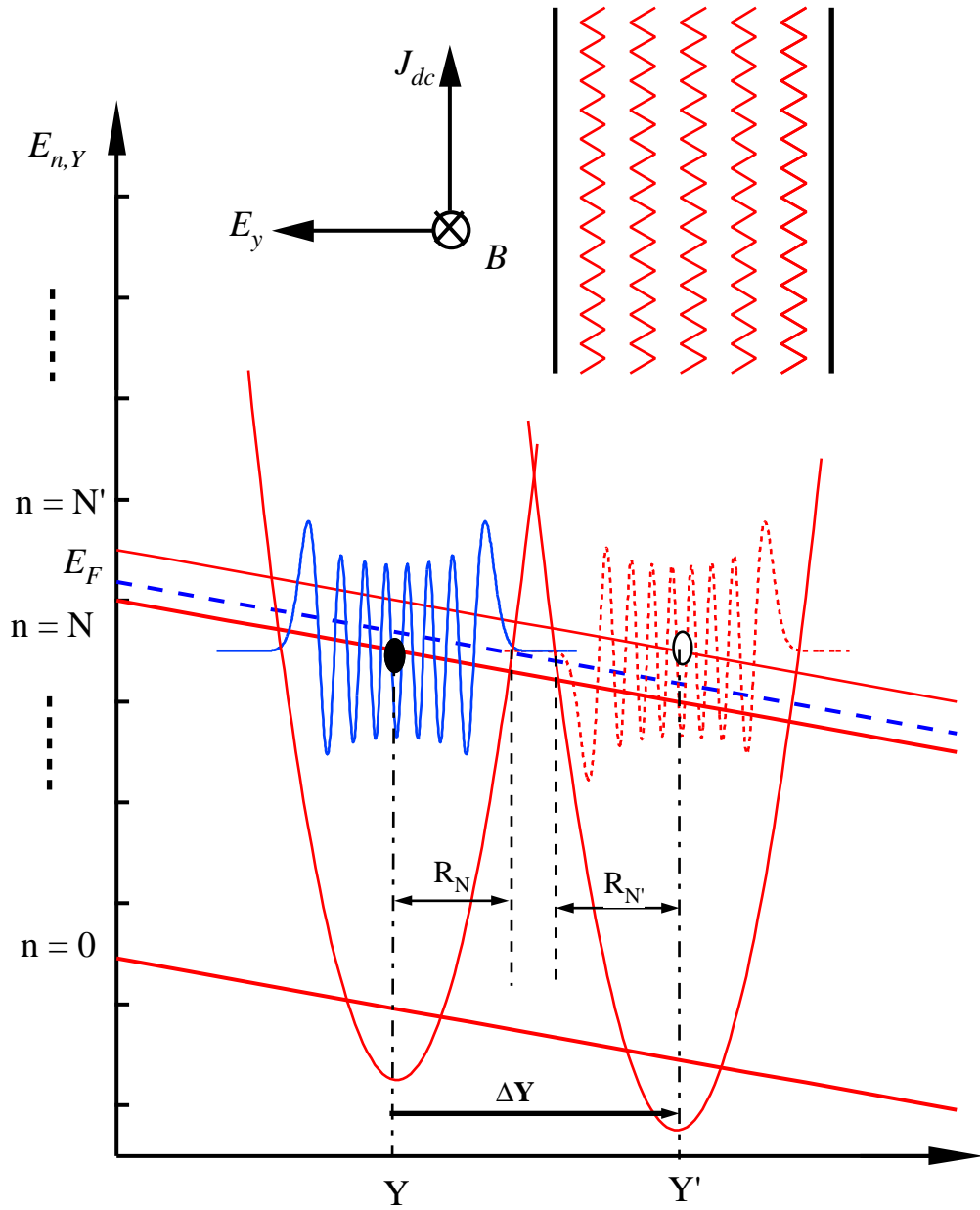
Figure 3.4. The Landau levels are spatially tilted along the direction of electric field (y direction), and the Fermi level has the same slope as the Landau levels. Elastic scattering cause the electron hopping between different Landau levels with a distance given by $\Delta Y = Y' - Y = l\hbar\omega_c/eE_y$. The vanishing of overlap between the oscillatory wave functions when $\Delta Y > R_N + R_{N'} \approx 2R_c$ means the maxmium hopping distance allowed is about $2R_c$. The configuration of the crossed electric and magnetic field is also shown.

The energy levels are given by (see Eq. 1.28)

$$E_{NY} = (N + \frac{1}{2})\hbar\omega_c - eE_yY + \frac{1}{2}m^*v_d^2. \tag{3.3}$$

Due to the electrostatic potential of the Hall field, the degeneracy of Landau levels with respect to k_x (or Y) is lifted and the Landau levels are tilted spatially along the Hall field E_y with a slope give by eE_y. Since the density of electrons is largely homogenous within the sample, the distribution function of the electrons should not depend on the guiding center Y [12], which means the Fermi level is also tilted along the y direction with the same slope as that of the Landau levels [31]. As a result, all the states within one Landau level with different guiding centers Y are equally occupied.

In the presence of elastic scattering, an electron may transfer a momentum $q_x = k_x - k'_x$ to a scatterer, which is equivalent to a hopping (migration of the guiding center) in the y direction at a distance $\Delta Y = Y' - Y = l_B^2 q_x$. This hopping gives a current density j_y [11, 12], hence a conductivity (see Eq. 1.36)

$$\sigma_{yy} = \frac{j_y}{E_y} = \frac{1}{E_y}\frac{e}{2L_xL_y}\sum_{\mu\mu'}W_{\mu\mu'}(Y' - Y)f_\mu(1 - f_{\mu'}), \tag{3.4}$$

where $\mu = (NY)$, $\mu' = (N'Y')$, L_x and L_y the dimensions of the 2DEG, $f_\mu = 1/(e^{(E_\mu - E_F)/k_BT} - 1)$ the Fermi distribution of the electrons, and $W_{\mu\mu'}$ the transition rate from the initial state $|\mu\rangle$ to final state $|\mu'\rangle$ in the Born approximation [13]:

$$\begin{aligned}
W_{\mu\mu'} &= \frac{2\pi}{\hbar}\frac{n_i}{L_xL_y}\sum_{q_x,q_y}|V(q)|^2|\langle\mu'|e^{i\vec{q}\cdot\vec{r}}|\mu\rangle|^2\delta(E_\mu - E_{\mu'}) \\
&= \frac{n_i}{\hbar L_xl_B}\delta(E_\mu - E_{\mu'})\int dQ_y\left|V\left(\frac{Q}{l_B}\right)\right|^2 J_N^l(Q), \tag{3.5}
\end{aligned}$$

where $Q \equiv ql_B = \sqrt{Q_x^2 + Q_y^2}$, $Q_x \equiv \Delta Y/l_B$, n_i is the density of the random scatterers, $V(q)$ is the effective Fourier component of the scatterring potential seen by the 2DEG, and [32]

$$J_N^l(Q) = \left|\int e^{iq_yy}\phi_N(y - Y)\phi_{N+l}(y - Y')\right|^2$$

$$= \frac{N!}{(N+l)!}\left(\frac{Q^2}{2}\right)^l e^{-\frac{Q^2}{2}}\left[L_N^l\left(\frac{Q^2}{2}\right)\right]^2, \qquad (3.6)$$

with $l = N' - N$ the index difference between involved Landau levels and $L_N^l(x)$ the generalized Laguerre polynomial.

Note that $W_{\mu\mu'} = W_{\mu'\mu}$ (this is generally true for *elastic* scattering), Eq. 3.4 can be rewritten as

$$\sigma_{yy} = \frac{j_y}{E_y} = \frac{1}{E_y}\frac{e}{2L_xL_y}\sum_{\mu\mu'}W_{\mu\mu'}(Y'-Y)(f_\mu - f_{\mu'}) \qquad (3.7)$$

In Eq. (3.5), the $\delta(E_\mu - E_{\mu'})$ accounts for the conservation of energy, which gives $eE_y\Delta Y = l\hbar\omega_c$. This means a electron hopping along y direction should cause a transition between Landau levels, and the hopping distance is determined by

$$\Delta Y_l = \frac{l\hbar\omega_c}{eE_y} = l\frac{\hbar}{m^*v_d} = l\frac{e\hbar n_e}{m^*J_{dc}}, \qquad (3.8)$$

which does not depend on the magnetic field, and is fixed for a given current density J_{dc}. The selection rule of Eq. (3.8) is unusual, in that it only stems from the two dimensional nature of the electrons.

The resistivity along the x direction (assume $\mu B \gg 1$) is $\rho_{xx} = \sigma_{yy}/(\sigma_{xx}\sigma_{yy} + \sigma_{xy}^2) \approx \rho_{xy}^2\sigma_{yy}$. By working out σ_{yy}, finally we get

$$\rho_{xx} = \frac{h}{e^2}\frac{(2\pi)^3 n_i m^{*4} v_d^2}{h^6 n_e^2}\sum_{Nl}(f_N - f_{N+l})P_{Nl}(Q_{xl}), \qquad (3.9)$$

with $Q_l \equiv \sqrt{Q_{xl}^2 + Q_y^2}$, $Q_{xl} \equiv \Delta Y_l/l_B$, and

$$P_{Nl}(Q_{xl}) = \frac{Q_{xl}^5}{l^4}\int dQ_y \left|V\left(\frac{Q_lQ_{xl}}{\Delta Y_l}\right)\right|^2 J_N^l(Q_l). \qquad (3.10)$$

The function $P_{Nl}(Q_{xl})$ can be numerically evaluated for a given $V(q)$. We simply assume a constant $V(q)$, which is good for short-range scattering, to calculate this function. The results show that P_{Nl} has a dominant maximum at the point

$$Q_{xl} = \gamma\sqrt{2N+1} \quad \text{with} \quad \gamma \approx 2.0. \tag{3.11}$$

The term $f_N - f_{N+l}$ in Eq. (3.9) means the transition should occur at the vicinity of Fermi level, i.e., we have $N \approx N_F$ where N_F is the Landau level index at the Fermi level, thus Eq. (3.11) is equivalent to

$$\Delta Y_l = Q_{xl}l_B = \gamma R_c \approx 2R_c, \tag{3.12}$$

where $R_c = \gamma\sqrt{2N_F+1}l_B = l_B^2\sqrt{2\pi n_e}$. Comparing with Eq. (3.8), the condition Eq. (3.12) leads to

$$B_l = \gamma\frac{\sqrt{2\pi}m^*}{e^2}\frac{1}{\sqrt{n_e}}\frac{J_{dc}}{l}, \tag{3.13}$$

which explains well the result of Eq. (1).

From the slopes of the fan diagram in Fig. 3.3, we obtain $\gamma = 1.72, 1.63, 1.88, 2.05$ for the Hall bars with width $w = 200, 100, 50, 20$ μm respectively. Such values, determinded experimentally, are close enough to the theoretical vale $\gamma \approx 2.0$, indicating the validity of our model even in a quantitative sense. Moreover, we measured the density dependence of the oscillation maxima, and plot the results in Fig. 3.5. It is clearly shown that peak positions $\propto 1/\sqrt{n_e}$.

The resonance condition Eq. (3.12) can be interpreted semiclassically as following. From Eq. (3.4), the conductivity σ_{yy} is proportional to the transition rate $W_{\mu\mu'}$ between two Landau levels near the Fermi level. The transition rate drastically goes to zero when $\Delta Y > R_N + R_{N'} \approx 2R_c$ because within this region there is almost no overlap between the oscillatory wave functions, as shown in Fig. 3.4. Thus the furthest distance the electron can hop is around $(\Delta Y)_{\max} \approx 2R_c$. Note that σ_{yy} is proportional to ΔY, so that naturally a conductivity peak appears at $\Delta Y = (\Delta Y)_{\max} \approx 2R_c$.

3.3 Discussions and conclusions

The hopping at a distance $2R_c$ along y direction is equivalent to a momentum transfer along x direction $\Delta k_x = 2R_c/l_B^2 = 2k_F$. It is interesting to point out
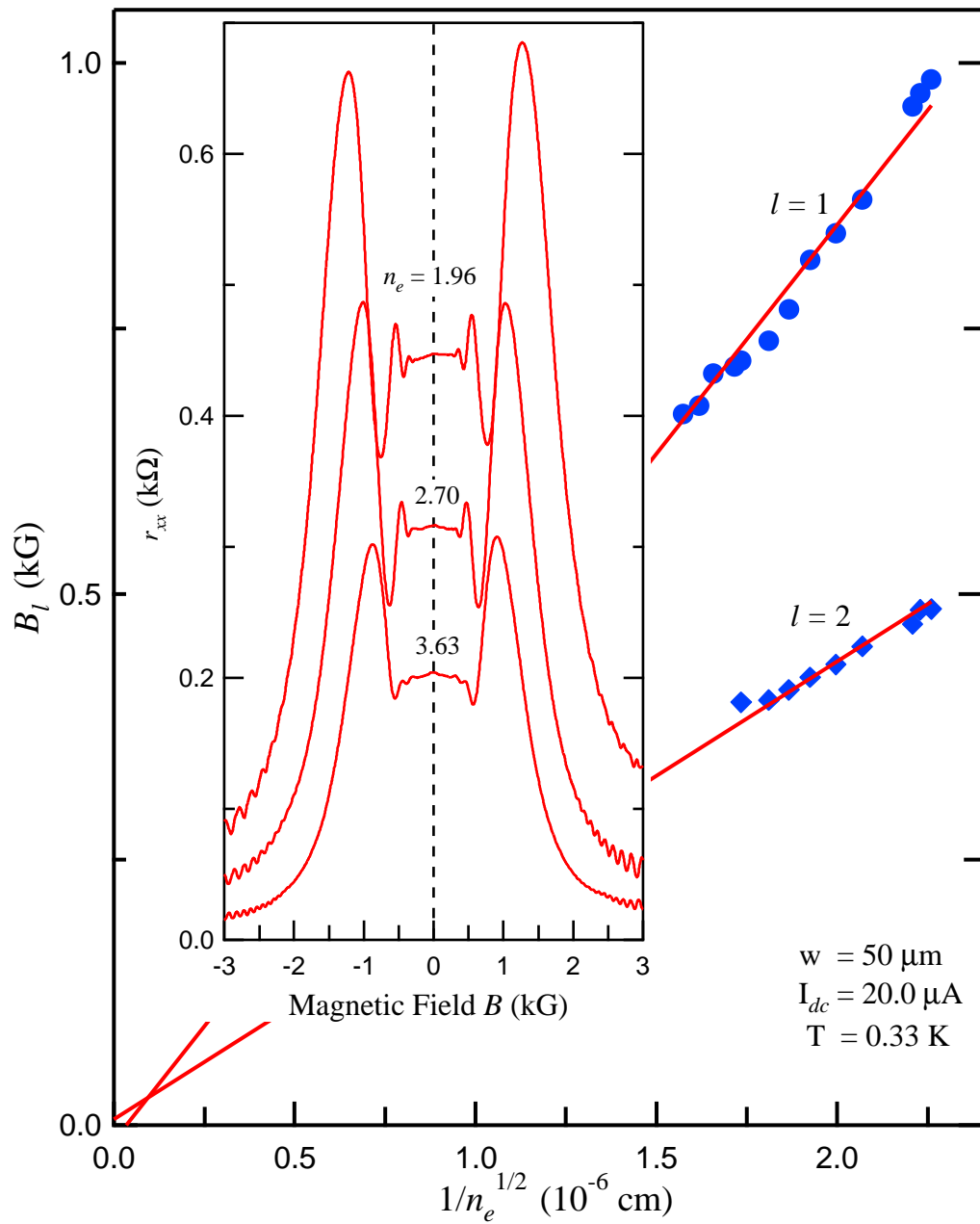
Figure 3.5. The density dependence measurement shows that the maximum positions are scaled as $1/\sqrt{n_e}$. The inset shows measured differential magnetoresistance traces at selected electron densities.

that a similar momentum transfer mechanism has been used to account for the magneto-acoustic-phonon resonance of a 2DEG [32].

In a high mobility 2DEG, the elastic scatters for electrons are mainly ionized impurities in the remote doping layer, residual background ionized impurities throughout the material, interface roughness, and neutral impurities in the GaAs well [33]. The remote ionized impurity scattering is long-ranged and in momentum space its potential is exponentially confined into a narrow range with a characteristic momentum $q_s \sim 1/d_s$ [34]. In our samples $d_s = 70\ nm$, equivalent to a $q_s \sim 0.014\ nm^{-1}$ which is much less than $2k_F \approx 0.22\ nm^{-1}$; therefore the remote ionized impurities are not likely to contribute to the oscillations. The other three mechanisms mentioned above are short-ranged, and therefore in principle could contribute to the oscillations we are discussing. The scattering length of the interface roughness and neutral scatters are both at atomic scale, so their potential seen by the 2DEG in momentum space are all almost constant within the scale of $2k_F$. Our numerical result of Eq. (3.12) is modeled on this fact. It is usually assumed that the remote ionized impurities are the main sources of scattering for 2DEGs in GaAs/AlGaAs heterostructures. However, for high mobility samples with wide spacer, the residual impurities and interface roughness become important [35, 36]. Indeed, according to a theoretical study [37], the negative magnetoresistance as shown in the $I_{dc} = 0\ \mu A$ trace of Fig. 3.1 is a strong evidence for the significance of such short-range scatterers in our samples.

In conclusion, we have observed a novel type of magnetoresistance oscillations in a laterally confined high-mobility 2DEG, which can be attributed to the spatial hopping of electrons between tilted Landau levels under a current induced Hall field. Strong short-range scattering is needed for this class of oscillations to occur.

3.4 Miscellaneous data on MZTR

3.4.1 Observing MZTR at fixed magnetic field by sweeping dc current

From Eq. 3.13, it is clear that the MZTR should also be observed in r_{xx} vs I_{dc} at fixed B except for in r_{xx} vs B at fixed I_{dc} (as shown in Fig. 3.1). This point is demonstrated in Fig. 3.6, where r_{xx} periodic in I_{dc} at fixed B is indeed observed.

3.4.2 MZTR observed on samples with higher mobility

More prominent MZTR has been observed in samples with higher mobility ($\mu > 1 \times 10^7$ cm^2/Vs). The MZTR is not only observed from the differential resistance (r_{xx}) but also directly from the dc resistance (R_{xx}). An example is shown in Fig. 3.7. We explain the more prominence of the MZTR in higher mobility samples by the increasing relative contribution from the short range scatterers.

3.4.3 Indication of the role of interface roughness on MZTR

In a front gated quantum well sample, initially the MZTR is very weak, however eventually this effect can be very strong by increasing the positive gate voltage, as shown in Fig. 3.8. We interpret this result as possible indication of the involvement of interface roughness, since more positive gate voltage will push the electrons more close to the interface, thus a larger contribution to the scattering from the interface roughness.
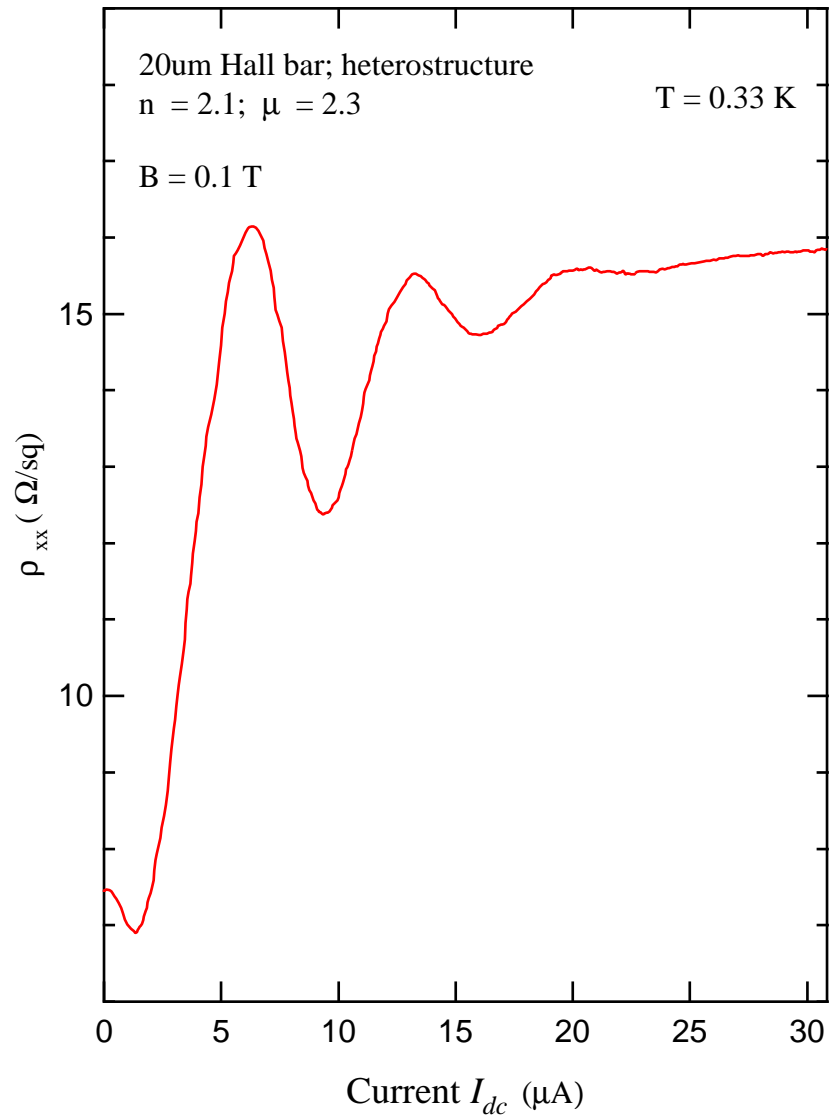
Figure 3.6. MZTR observed through r_{xx} vs I_{dc} at fixed B.
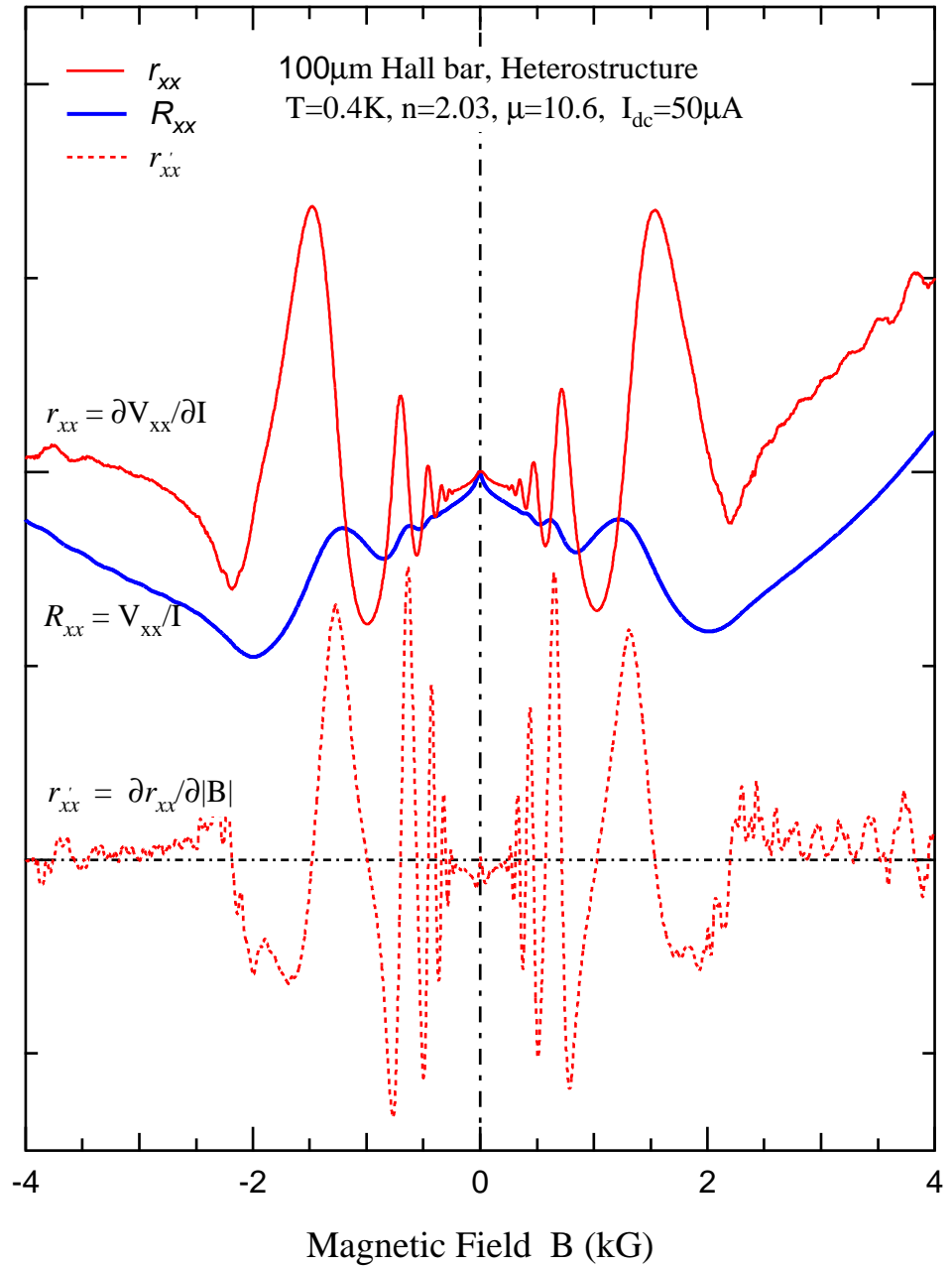
Figure 3.7. MZTR observed in a GaAS/Al$_{0.3}$Ga$_{0.7}$As heterostructure with $n_e = 2.03 \times 10^{11}$ cm^{-2} and $\mu = 10.6 \times 10^6$ cm^2/Vs. The MZTR is very strong in differential trace (r_{xx}) as well as in dc trace (R_{xx}). The effect in this sample is much more prominent than that shown in Fig. 3.1 where the sample mobility is $\mu \approx 3 \times 10^6$ cm^2/Vs.
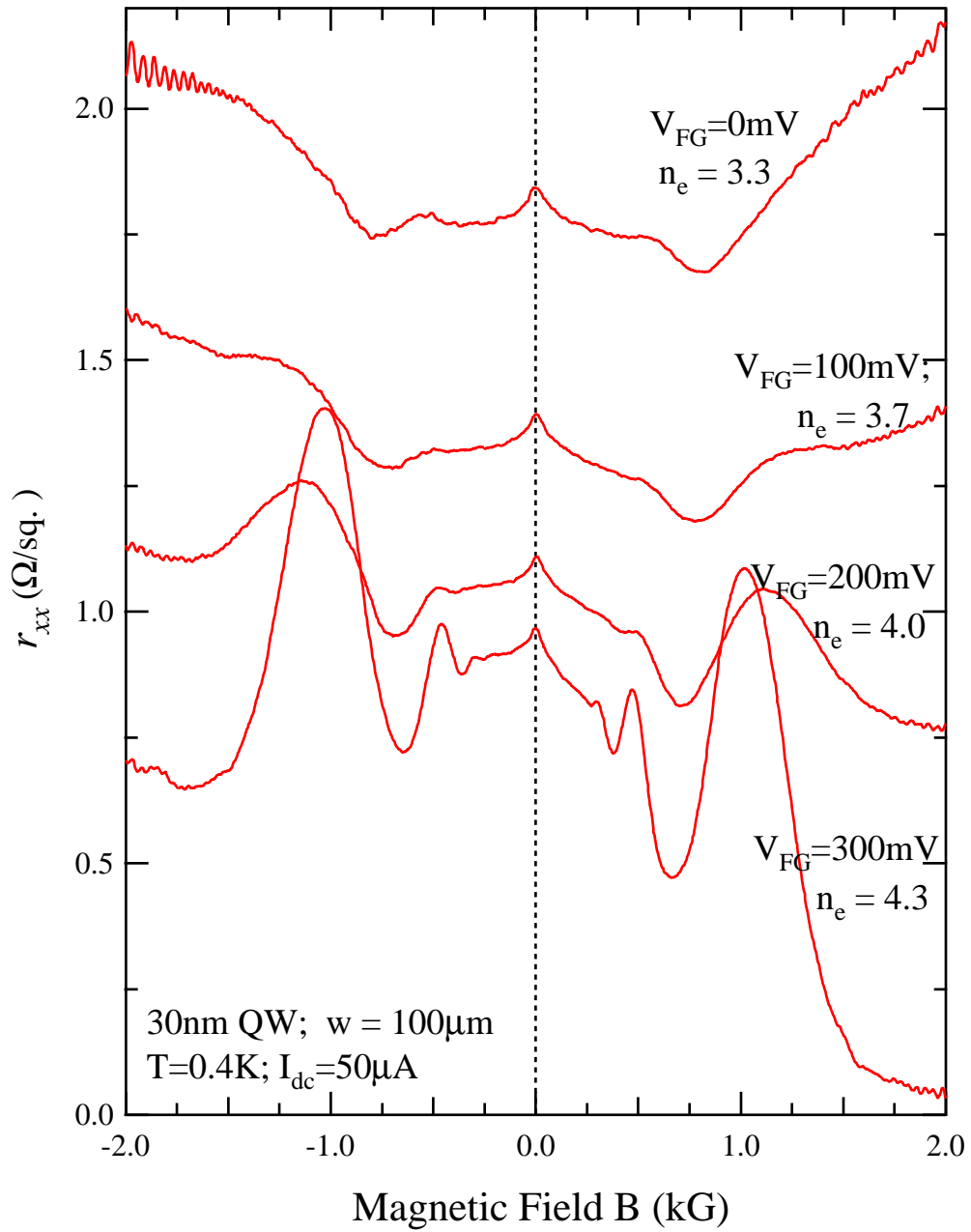
Figure 3.8. MZTR observed in a gated $_{0.24}Ga_{0.76}As/GaAs/Al_{0.24}Ga_{0.76}As$ quantun well. Initially the MZTR is rather weak, but eventually it becomes very strong by applying a positive gate voltage.

CHAPTER 4

MAGNETO OSCILLATIONS INDUCED BY
MICROWAVE AND THE EMERGENCE
OF THE ZERO-RESISTANCE OR
ZERO-CONDUCTANCE STATE

Interesting new phenomena in dc transport can arise in a high-mobility two-dimensional electron system (2DES) when it is subjected to microwave (MW) radiation [3, 4, 5, 38]. Giant MW photoconductivity oscillations (in $1/B$, the inverse magnetic field) were originally observed in a 2DES in GaAs/Al$_x$Ga$_{1-x}$As heterostructures with a mobility $\sim 3 \times 10^6$ cm^2/Vs [3, 38]. In samples of a very high mobility (typically $> 1 \times 10^7$ cm^2/Vs), a remarkable "zero-resistance state" (ZRS) emerges from the oscillation minima [4, 5]. The discovery of MW-induced magneto oscillations and the ZRS has stimulated considerable current theoretical interest [39, 40, 41, 42, 43, 44, 45, 46].

Corresponding to the ZRS in samples with Hall bar geometry, we have also observed a "zero-conductance state" (ZCS) in samples with Corbino geometry [20]. We demonstrated that, regardless of the presence of the MW fields, the conductance and resistance are invertible according to a standard dc transport tensor relation; hence, the observed ZCS is equivalent to ZRS. This observation indicates that the ZRS (ZCS) behaves like an *insulator* rather than a *superconductor* as proposed in Ref. [5].

In this chapter, Sec. 4.1 and 4.2 describe the observations of the MW-induced oscillatory magnetoresistance and the subsequent ZRS associated with the oscillation minima. Sec. 4.3 concentrates on our experimental observation of the ZCS,

which reveals the insulator nature of the ZRS (ZCS). Some theoretical explanations will be given in Sec. 4.4.

4.1 Observations of microwave-induced photoconductivity resonance

The microwave-induced photoconductivity resonance (MIPCR) was firstly observed by Zudov *et al.* [47] in 1997 in a systematic study of the photoresistence of a 2DES under crossed microwave and weak magnetic fields. As an example, Figure 4.1 shows photoresistance traces measured on a heterostructure sample with the electron density, $n_e \approx 2.0 \times 10^{11} cm^{-2}$, and mobility, $\mu \approx 3 \times 10^6$ cm^2/Vs. The remarkable MW-induced oscillations are found to be controlled by the ratio between the MW frequency (ω) and the cyclotron frequency (ω_c):

$$\epsilon \equiv \frac{\omega}{\omega_c} = \begin{cases} j & \text{maxima} \\ j + 1/2 & \text{minima} \end{cases} \quad j = 1, \ 2, \ 3, \ .... \tag{4.1}$$

Although the resonant photoconductivity associated with cyclotron resonance (refer to the peak at $\epsilon = 1$) was well known in the literature, the observation of oscillatory photoresistance was considered a surprise. Not only the observation of high order peaks ($\epsilon > 1$) but also the large amplitude was completely unexpected. Similar oscillatory photoresponse with even higher amplitude was subsequently observed by Ye *et al.* [38], using lower frequency microwaves (4–40 GHz) guided by transmission lines.

4.2 Toward the zero-resistance state – role of the electron mobility

Concurrent with the MIPCR, the photo signal (defined by the change of the resistance due to applying microwave) alternates in sign, specifically, the MW contribution to resistance is positive at the maxima and negative at the minima. Moreover, it was noticed that with higher sample mobility, the amplitude of the oscillations is larger and consequently the oscillation minima are closer to zero
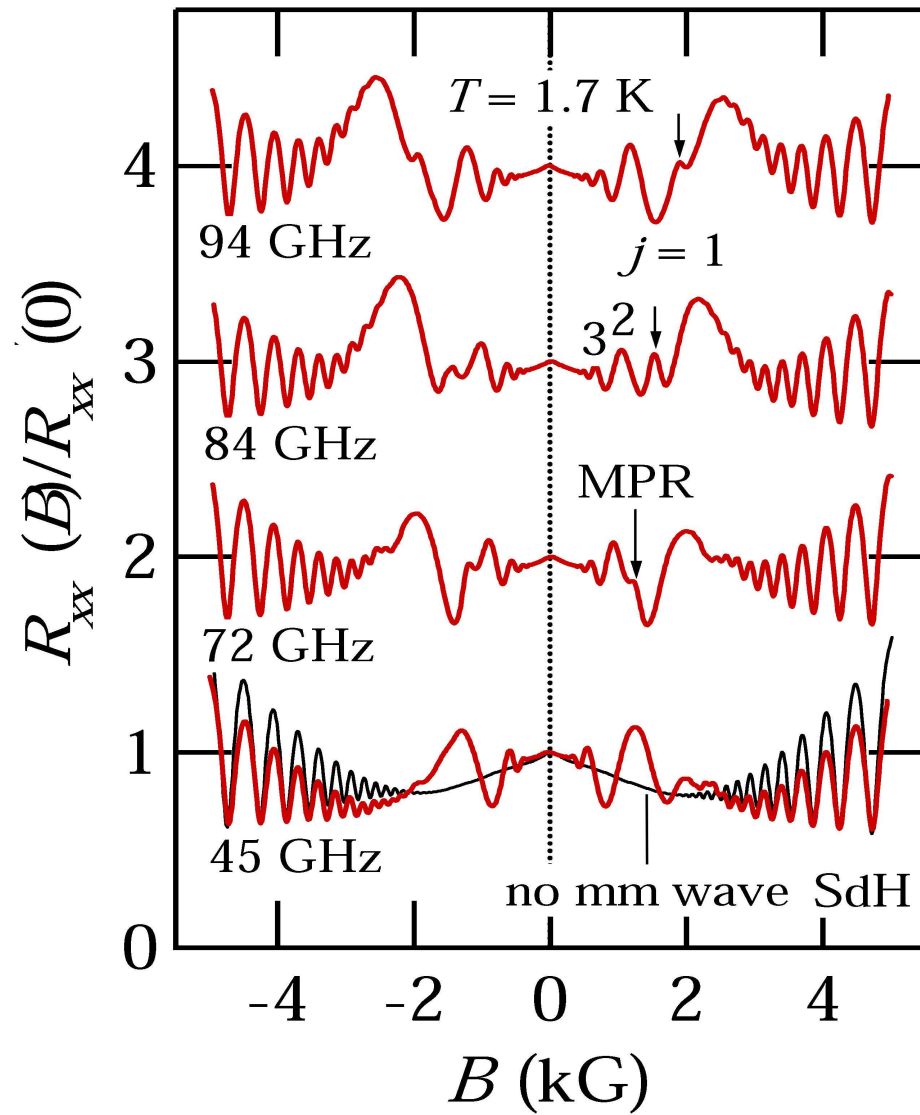
Figure 4.1. Oscillatory microwave photoresistance observed in a sample with mobility $\mu \approx 3 \times 10^6$ cm^2/Vs. For clarity, traces are vertically shifted in steps of 1.0. [Adapted from Ref. [3].]

under similar experiment conditions. This naturally leads to the speculation that the minima would ultimately reach zero in samples with very high mobility.

To explore the possibility of a "zero-resistance state" (ZRS) in the MIPCR minima, extensive surveys were pursued on the MIPCR by our group utilizing various samples. The initial evidence for the existence of the ZRS was obtained by Yang *et al.* in October 2000, from a 2DES with $\mu \approx 10 \times 10^6$ cm^2/Vs. As shown in Fig. 4.2, in addition to very strong MIPCR oscillations, the first oscillation minimum, at negative B side, indeed reaches zero when microwave frequency $f > 70 GHz$. Although the overall quality of this sample is not good enough to be conclusive, data shown in in Fig. 4.2 had indeed indicated an inceptive ZRS.

Eventually, in spring 2001, solid evidences for the ZRS were obtained by Zudov *et al.* from a 2DES with an ultrahigh mobility $\mu \approx 25 \times 10^6$ cm^2/Vs [4, 48]. A typical photoresistance trace R_{xx} is shown in Fig. 4.3. This trace shows very strong and sharp oscillations up to many orders ($\epsilon > 10$), and most strikingly, the emergency of wide, apparently zero-resistance, regions at the first three oscillation minima. At first glance, this R_{xx} trace resembles remarkably those of IQHE, but the R_{xy} trace, also shown in Fig. 4.3, is essentially classical, without showing quantization in the zero-resistance regimes. Typical residual resistances at the major minima are within $\pm 0.01\Omega$, roughly the noise level of the experiment. Moreover, the temperature dependence of the resistances at these minima shows a thermally activated behavior, $R_{xx}(T) \propto exp-T_0/T$, hence they would ultimately become zero at $T = 0$ [4]. This is the physical meaning of the term "zero-resistance state" used for this phenomenon. Although the experimental evidences for the ZRS were quite clear then, the underlying physics of the ZRS remained elusive due to the fact that even a theoretical explanation for the MIPCR was not available for quite a while.

The ZRS was independently reported also by Mani *et al.* and was initially interpreted by them as evidence for superconductivity [5].
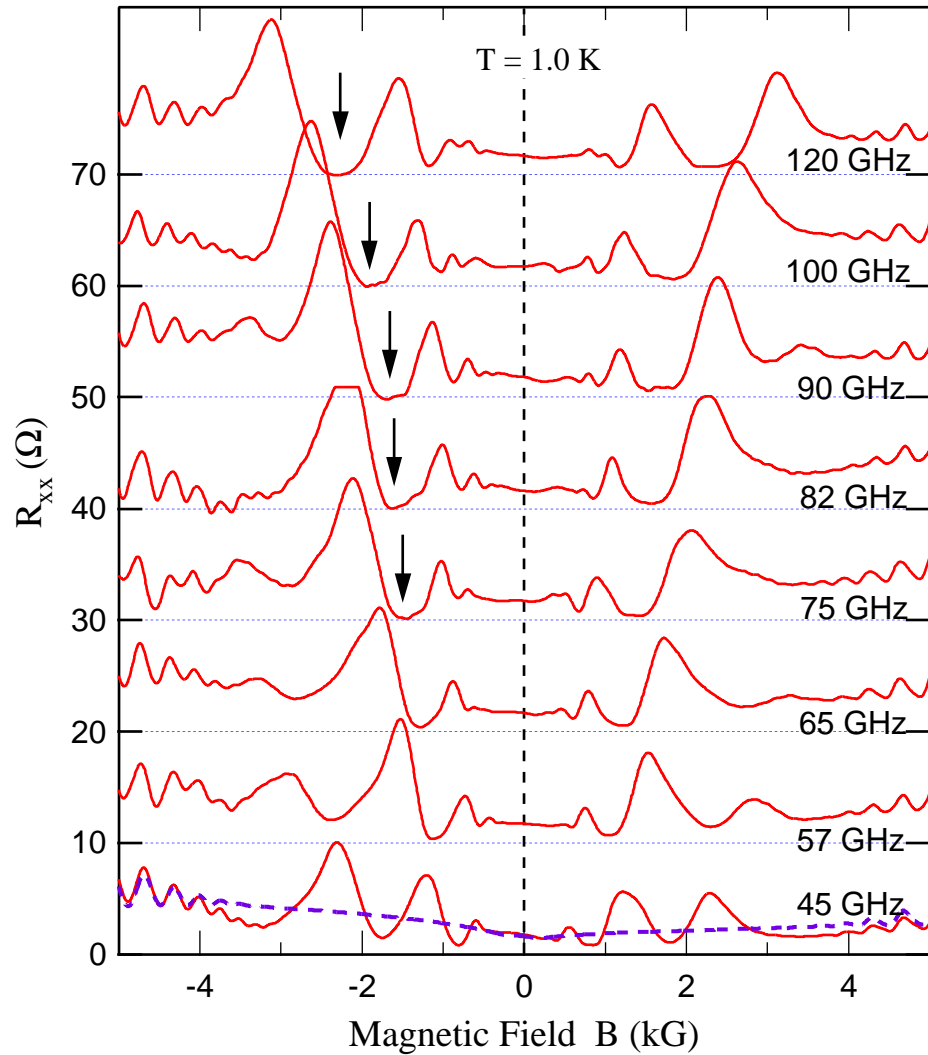
Figure 4.2. MIPCR oscillations observed in a aAs/Al$_{0.3}$Ga$_{0.7}$As heterostructure sample of $n_e \approx 2.7 \times 10^{11}$ cm^{-2} and $\mu \approx 10 \times 10^6$ cm^2/Vs. As indicated by arrows, the first oscillation minimum (at negative B side) touches zero when microwave frequency $f > 70$ GHz, indicating an inceptive zero-resistance state there.
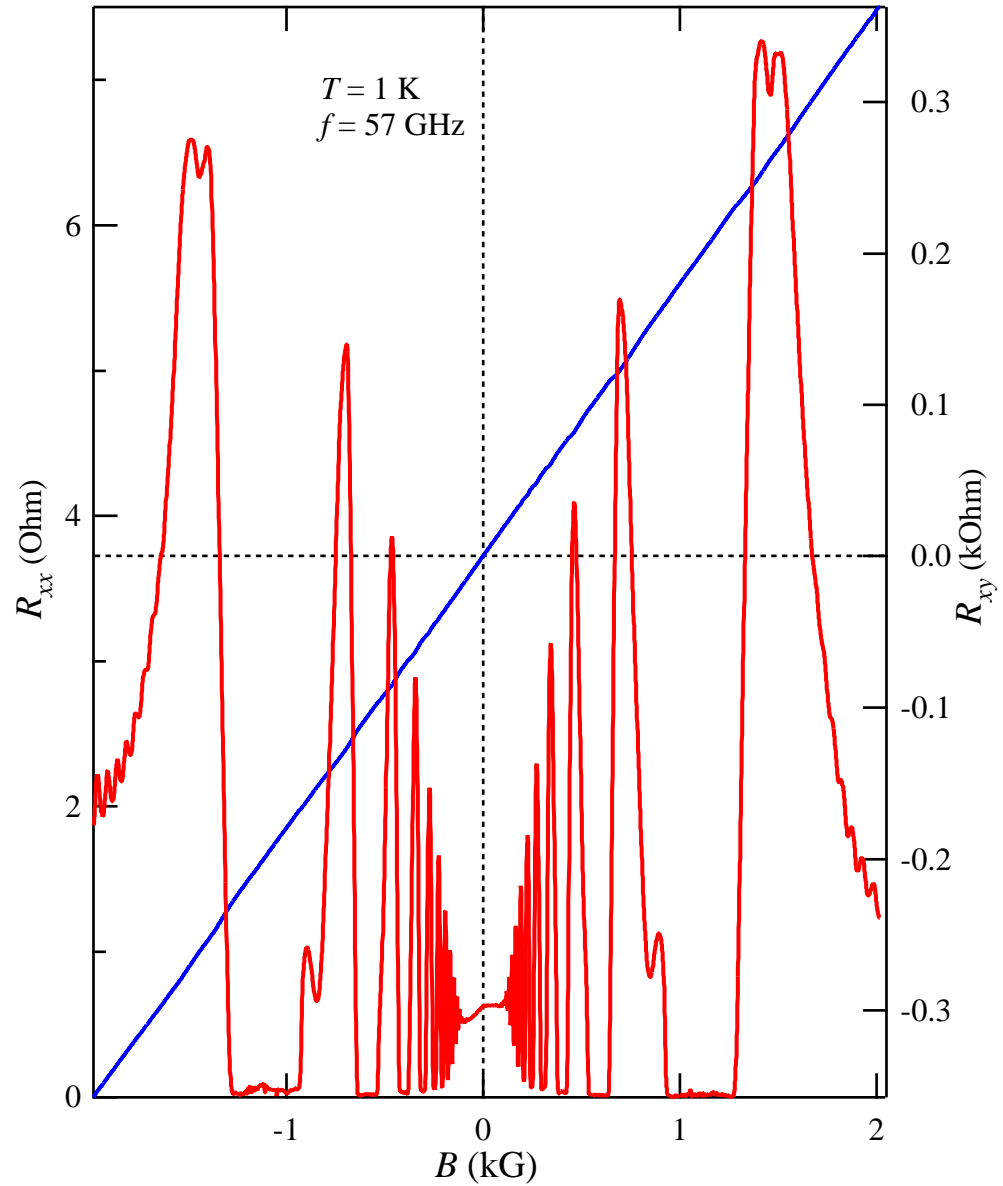
Figure 4.3. The ZRS observed on a $Al_{0.24}Ga_{0.76}As/GaAs/Al_{0.24}Ga_{0.76}As$ quantum well, with $n_e \approx 3.5 \times 10^{11}$ cm^{-2} and $\mu \approx 25 \times 10^6$ cm^2/Vs. [M. A. Zudov, R. R. Du, L. N. Pfeiffer, and K. W. West (traces taken in spring 2001, published in Ref. [48]).]

4.3 The observations of MW-induced zero-conductance state

A general feature of the 2DES transport is that the resistivity and conductivity are fundamentally related. It is well known [49] that, in the quantized Hall effects, a vanishing diagonal resistivity (ρ_{xx}) is equivalent to a vanishing conductivity (σ_{xx}) and these two quantities relate to each other by

$$\sigma_{xx} = \rho_{xx}/(\rho_{xx}^2 + \rho_{xy}^2) \approx \rho_{xx}/\rho_{xy}^2 = (n_e e/B)^2 \rho_{xx}, \qquad (4.2)$$

where n_e is the electron density.

Experimentally, it remained unclear whether Eq. 4.2 holds for the microwave-induced oscillations and the subsequent ZRS. This question is relevant, in particular, to the understanding of the nature of the ZRS.

To address the above question, we performed direct conductivity measurements utilizing Corbino samples of a high-mobility 2DES. We have observed MW-induced vanishing dc *conductance* state, corresponding to ZRS. Such a state is termed "zero-conductance state" (ZCS) in the context of its thermally activated behavior. The experiments demonstrate that, regardless of the presence of the MW fields, the conductance and resistance are invertible according to Eq. (1), up to a scaling factor; hence, the observed ZCS is equivalent to ZRS. Macroscopically, the 2DES behaves like an insulator in ZCS regime. Such an observation imposed constraints on theoretical models of ZRS, for example, the superconductivity origin for the ZRS is ruled out because of the equivalence between ZRS and ZCS.

4.3.1 Samples and experimental setup

Our samples were cleaved from a $Al_{0.24}Ga_{0.76}As/GaAs/Al_{0.24}Ga_{0.76}As$ quantum well (QW) wafer grown by molecular beam epitaxy. The width of the QW is 25 nm and the electrons are provided by Si δ-doping layers 80 nm above and below the QW. After illumination by a red light-emitting diode at $T \approx 1.5$ K, the electron density, n_e, and mobility, μ, reached 3.55×10^{11} cm^{-2} and 12.8×10^6 cm^2/Vs, respectively. The Corbino samples, with an inner diameter $d_1 \approx 0.5$ mm and an

outer diameter $d_2 \approx 3.0$ mm, were made on a ~ 4 mm$\times 4$ mm square. Ohmic contacts were made of indium. To compare the conductance measurement with a resistance measurement, a ~ 4 mm$\times 4$ mm square sample (from the same wafer) was made with eight indium contacts placed along the perimeter.

The experimental setup is shown in Fig. 4.4. Except for the I–V characteristics, the conductance or resistance traces were recorded employing a low-frequency (2.7 Hz) lock-in technique while the sample was immersed in ^{3}He liquid and under continuous microwave irradiation of fixed frequency, f, and power, P.

The diagonal conductance, $G_{xx} = I/V$, of the Corbino sample was obtained by measuring the current (I) passing through the 2DES, while applying a voltage (V) between the inner and outer contacts. Here x denotes the direction along the radius. A typical bias of $V \sim 1$ mV was used for the measurements. The inset of Fig. 4.5 shows a schematic circuit of the measurement.

Without the MWs and while sweeping the magnetic field, the G_{xx} trace shows sequentially, in Fig. 4.5, a Drude conductance around $B = 0$, sharp Shubnikov–de Haas oscillations at $B \gtrsim 1.5$ kG, and the integer quantum Hall effect (IQHE) minima at $B \gtrsim 10$ kG. The trace is strictly symmetrical with respect to $B = 0$, indicating that the recorded G_{xx} is essentially free of mixture with the Hall conductance. Altogether, such standard dc transport attests to an exceptional quality of the Corbino sample. We note that at this temperature a residual conductance in the IQHE remains measurable. For example, at Landau level filling factor $\nu = 4$, its value is typically $\lesssim 5 \times 10^{-7}$ S, which is $\sim 10^{-7}$ of the conductance at $B = 0$. Finite residual conductance in the IQHE is commonly attributed to thermally activated conduction [50] or variable-range hopping conduction [51]

4.3.2 Conductance oscillations and the zero-conductance state

Figure 4.6 shows a G_{xx} trace with MW $f = 57$ GHz and with an incident power $P \approx 10$ μW on the sample surface. Notice that the temperatures marked in both Fig. 4.5 and Fig. 4.6 are those measured in the ^{3}He liquid. Strong MW induced
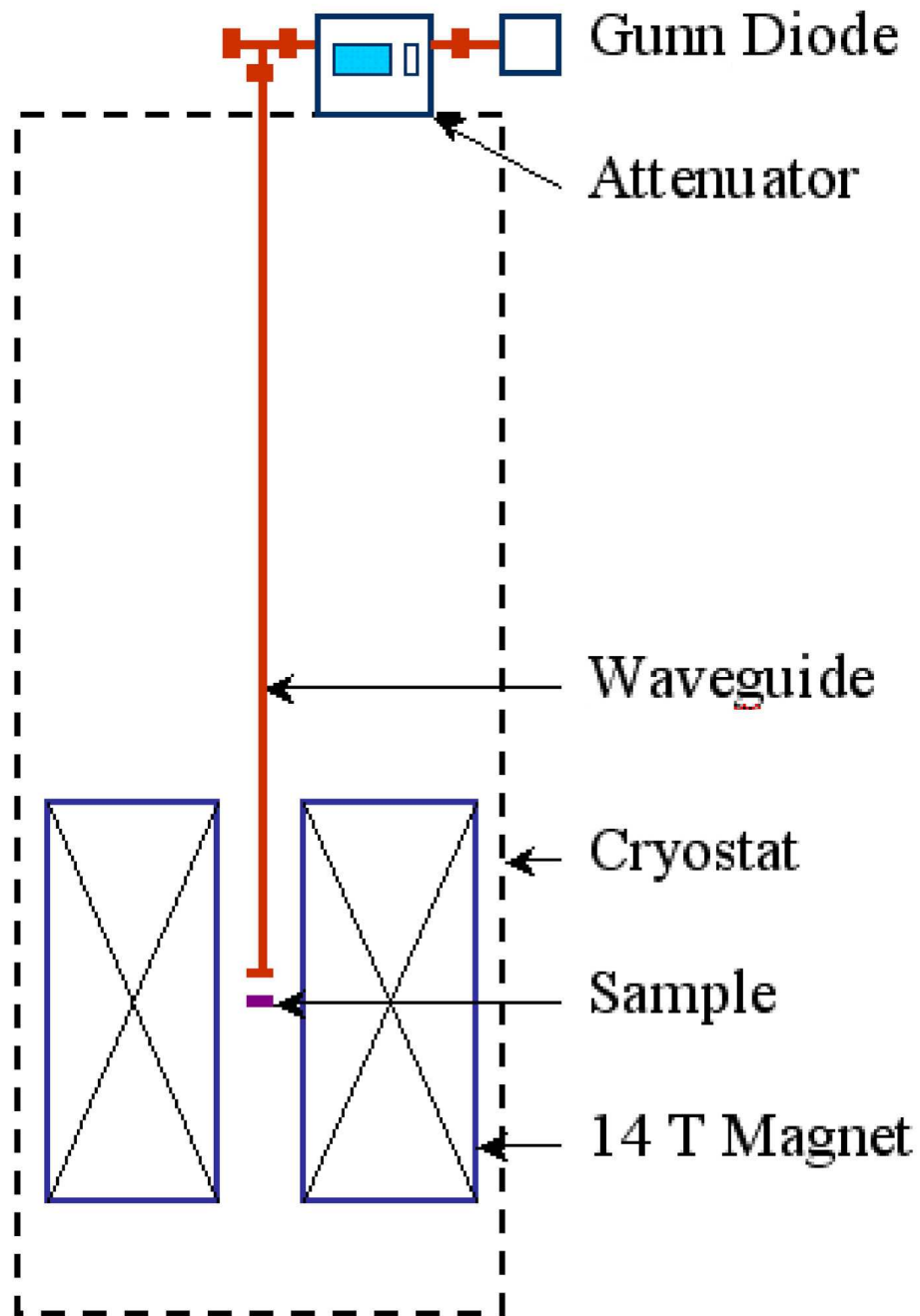
Figure 4.4. Setup for measuring microwave photoresponse of a 2DES: The measurements were performed in a sorption-pumped ^{3}He cryostat equipped with a superconducting magnet. The microwaves were generated by Gunn diodes and guided down to the sample (Faraday configuration) via an oversized (WR-28) waveguide.
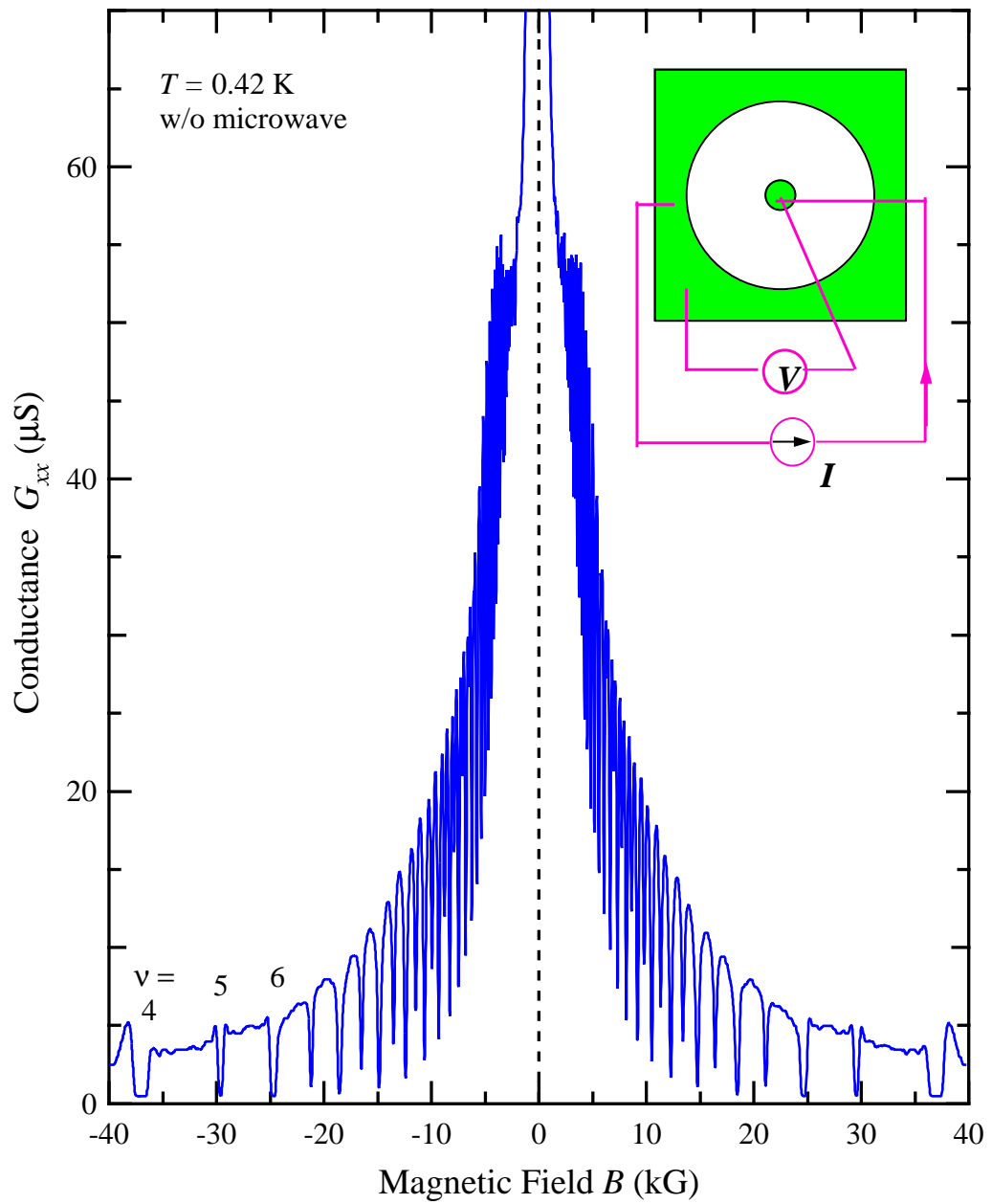
Figure 4.5. Magnetoconductance of a Corbino sample (without MW irradiation) is shown to exhibit sharp SdH oscillations at low magnetic field and flat IQHE minima at high magnetic field. The inset depicts the geometry of the sample and the measurement circuit.
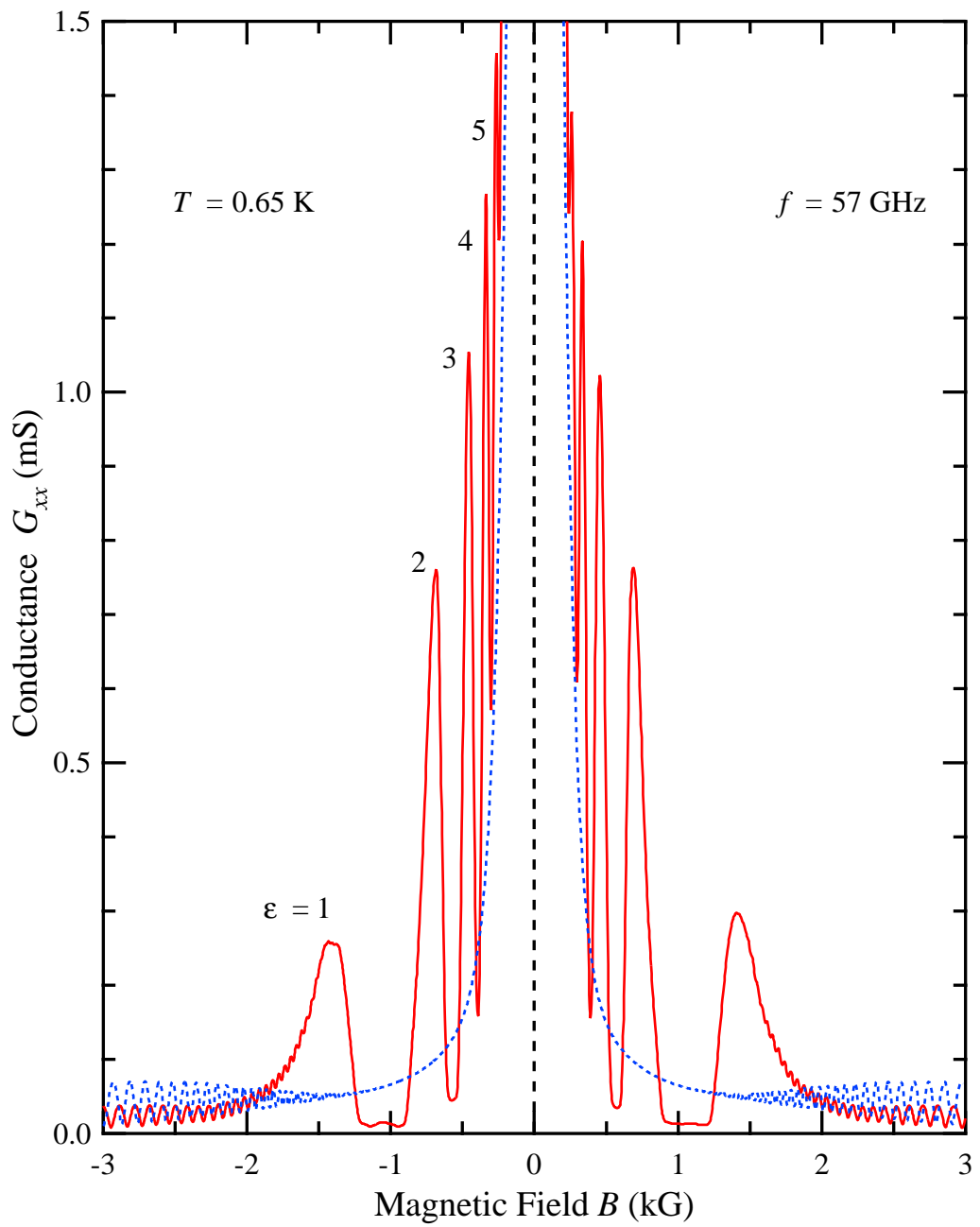
Figure 4.6. The conductance oscillations observed in the Corbino sample with microwave irradiation. A "zero-conductance state" at the first minimum is observed. A trace without MW irradiation (dotted line) is also presented for comparison.

conductance oscillations up to 5 orders are observed. The peaks are marked by $\varepsilon \equiv \omega/\omega_c = 1,\ 2,\ 3,\ \ldots$, where $\omega_c = eB/m^*$ is the cyclotron frequency, $m^* = 0.068\,m_e$ is the effective mass of the electron, and $\omega = 2\pi f$.

Our central finding from such measurements, however, concerns the "zero-conductance state" observed at the lowest oscillation minimum, around $B = \pm 1.05$ kG. This minimum spans a wide range of Landau level filling factors, $\nu = n_e h/eB$, from $\nu \sim 160$ to $\nu \sim 120$. Similar to the resistance measured in the ZRS, the conductance in the ZCS is found to be thermally activated. The temperature-dependent conductance at $B = 1.05$ kG (the center of the lowest minimum), corresponding to two different MW power levels, is shown in Fig. 4.7 and 4.8. The activated conductance spans almost one decade and can be reasonably fitted by an exponential dependence $G_{xx} \propto \exp(-T_0/T)$, with an activation energy $T_0 \approx 4.5$ K (9.3 K) for $P \approx 10$ μW (100 μW). Comparing the value 9.3 K with the $T_0 \approx 20$ K measured under a similar magnetic field and MW power, but in the ZRS of a cleaner sample [4], we interpret that the activation energy in this regime strongly correlates with the sample mobility.

On the other hand, we observed a drastic departure from the activated behavior in the lower temperature regime $T < 1$ K (2 K) for power level $P \approx 10$ μW (100 μW). In particular, the conductance becomes flat at reduced temperatures, rendering a residual conductance, $G_{xx} \lesssim 2 \times 10^{-5}$ S, at the lowest T of the experiment, $T \approx 0.65$ K. The above observation of a temperature independent residual conductance has been confirmed by separate measurements performed in a dilution refrigerator, where the lowest T of 170 mK can be attained with $f = 30$ GHz and $P \sim 100$ μW.

While at this stage the origin of the residual conductance remains to be clarified, two possible mechanisms can be proposed here: a) electron heating due to the MW irradiation, b) a parallel conduction channel created by MW excitation. In fact, we observed an enhanced residual conductance at $\nu = 4$ IQHE (from 5×10^{-7} S to 20×10^{-7} S) due to MW irradiation, as shown in Fig. 4.9.
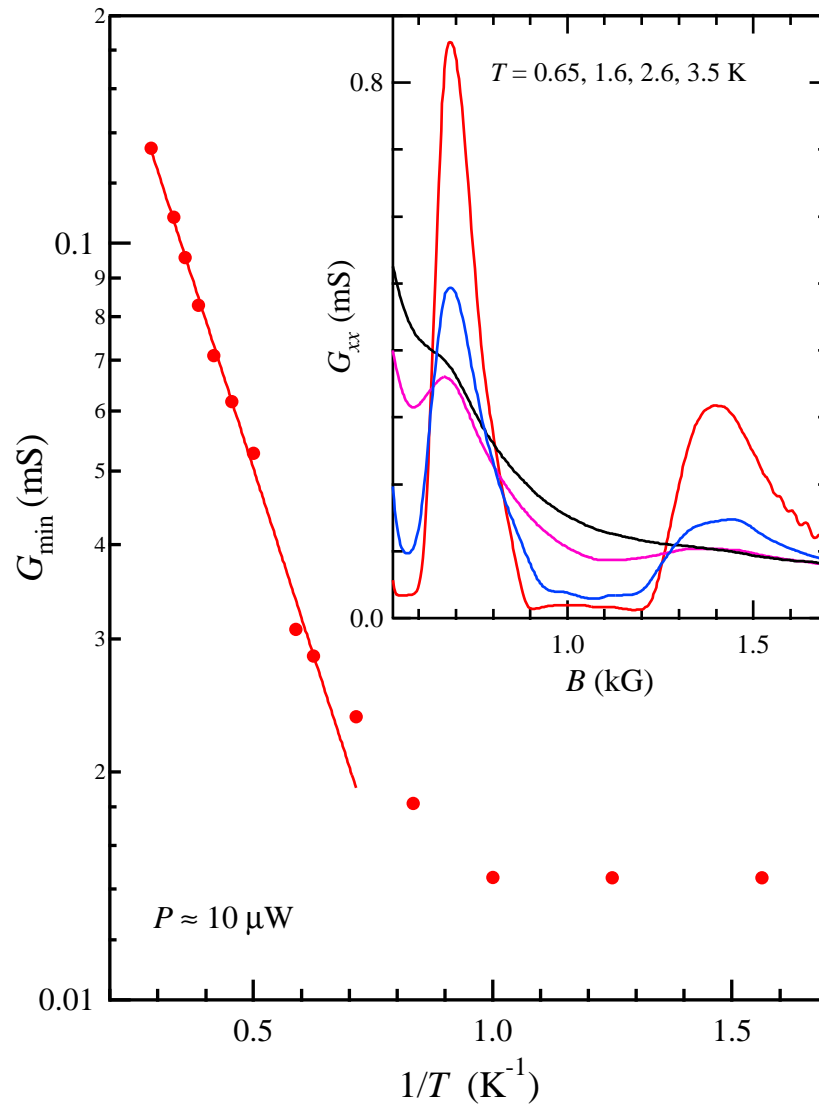
Figure 4.7. The conductance at the center of the first minimum for $f = 57$ GHz with $P \approx 10$ μW, plotted against $1/T$. The inset shows the conductance traces around the minimum at selected temperature. Solid lines represent fits to $G_{xx}(T) \propto \exp(-T_0/T)$.
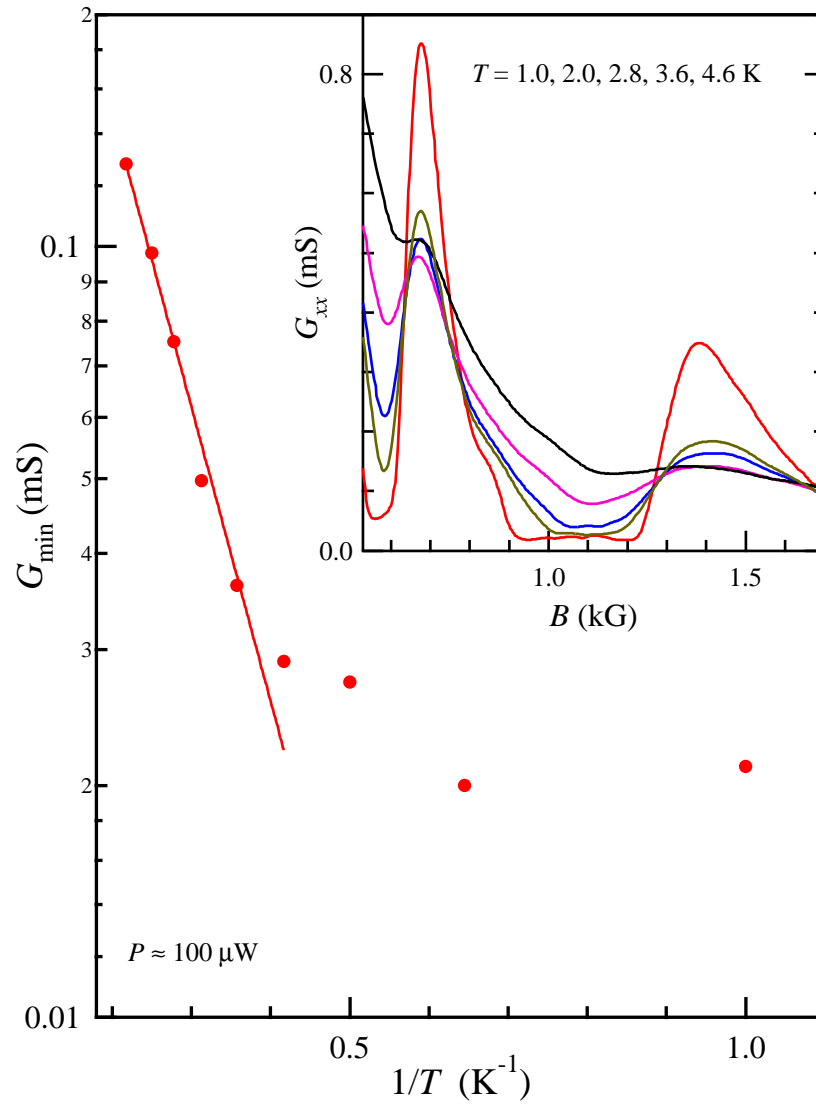
Figure 4.8. The conductance at the center of the first minimum for $f = 57$ GHz with $P \approx 100$ μW, plotted against $1/T$. The inset shows the conductance traces around the minimum at selected temperature. Solid lines represent fits to $G_{xx}(T) \propto \exp(-T_0/T)$.
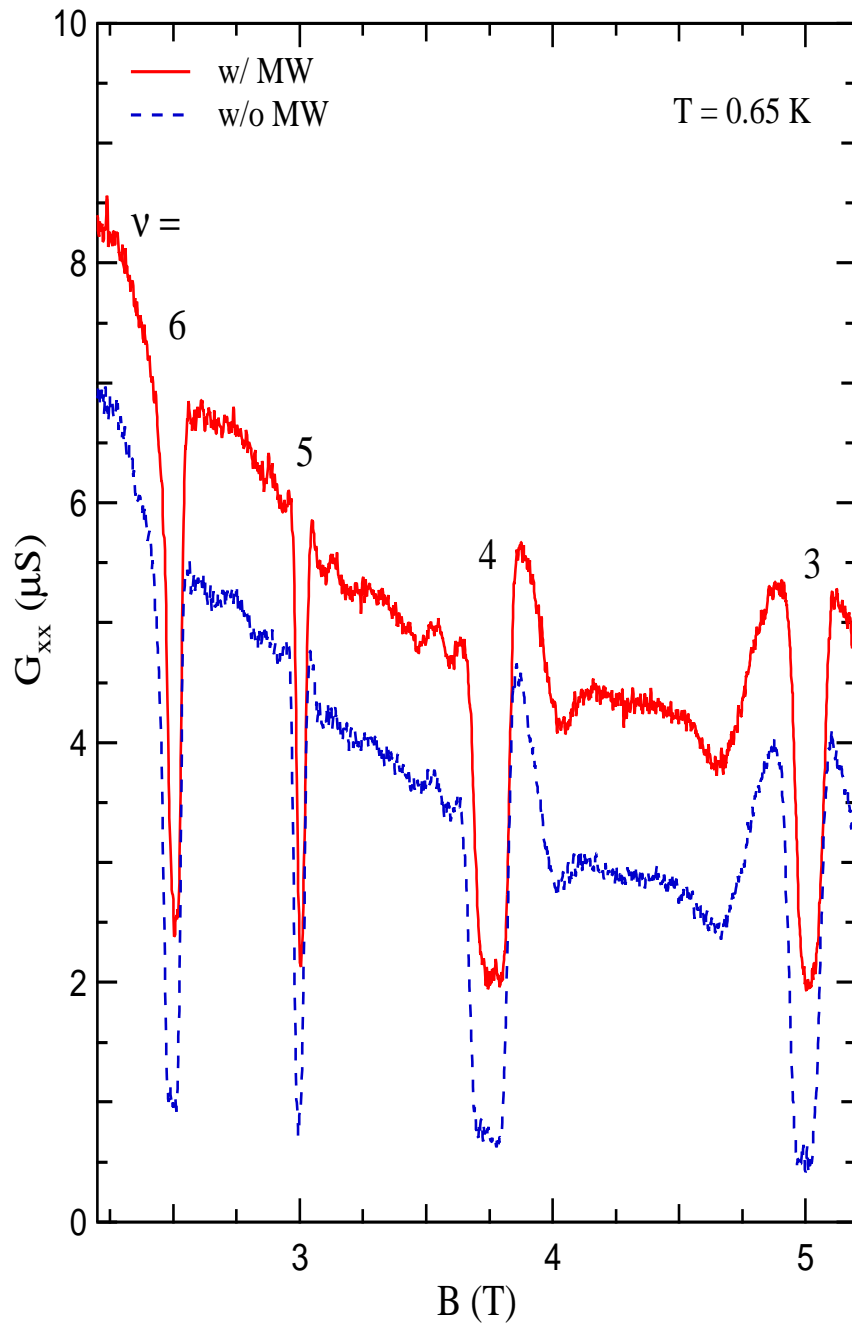
Figure 4.9. MW-Enhanced residual conductance for IQHE around $\nu = 3,\ 4,\ 5,\ 6$.

It is interesting to compare the residual *conductivity* in the ZCS with the conductivity quantum e^2/h. Considering the geometric factor of the Corbino sample and assuming a uniform distribution of the electric current passing through the contacts, we estimate a residual conductivity $\lesssim 6 \times 10^{-6}$ S, which is much less than e^2/h. We therefore conclude that the 2DES behaves like an insulator in the ZCS regime.

4.3.3 Invertibility between the MW-induced conductance and resistance – equivalence between the ZCS and ZRS

In order to compare the MW-induced conductance oscillations with the resistance oscillations, we calculate a diagonal conductance (G'_{xx}) from a diagonal resistance (R_{xx}) measured on a square sample, using the inversion relation $G'_{xx} \approx R_{xx}/\rho_{xy}^2 = (n_e e/B)^2 R_{xx}$. The quantity that can be directly compared between different samples is not the conductance but the conductivity. Since the conductivity is proportional to the conductance, we can normalize the conductance to a specific point B_0 (e.g., the first maximum of the oscillations), and compare the normalized conductances g_{xx} $[\equiv G_{xx}(B)/G_{xx}(B_0)]$. Figure 4.10 displays both the g_{xx} measured from the Corbino sample and the g'_{xx} converted from R_{xx} measured on a square sample. The R_{xx} of the square sample, measured under the same conditions as the G_{xx} ($T = 0.65$ K, $f = 57$ GHz, $P \approx 10$ μW), is also shown in Fig. 4.10. Slight asymmetry of the R_{xx} with respect to $B = 0$ might indicate a weak mixing of resistance tensor elements. Excellent agreement between the g_{xx}'s clearly demonstrates that under MW irradiation the dc conductance and resistance remain invertible up to a scaling factor.

4.3.4 I–V characteristics in the ZCS regime

We have also measured the I–V characteristics in the ZCS regime. In order to establish a constant bias voltage (V) across the contacts of the Corbino sample, a dc voltage was applied and the dc current (I) was measured using a current amplifier.
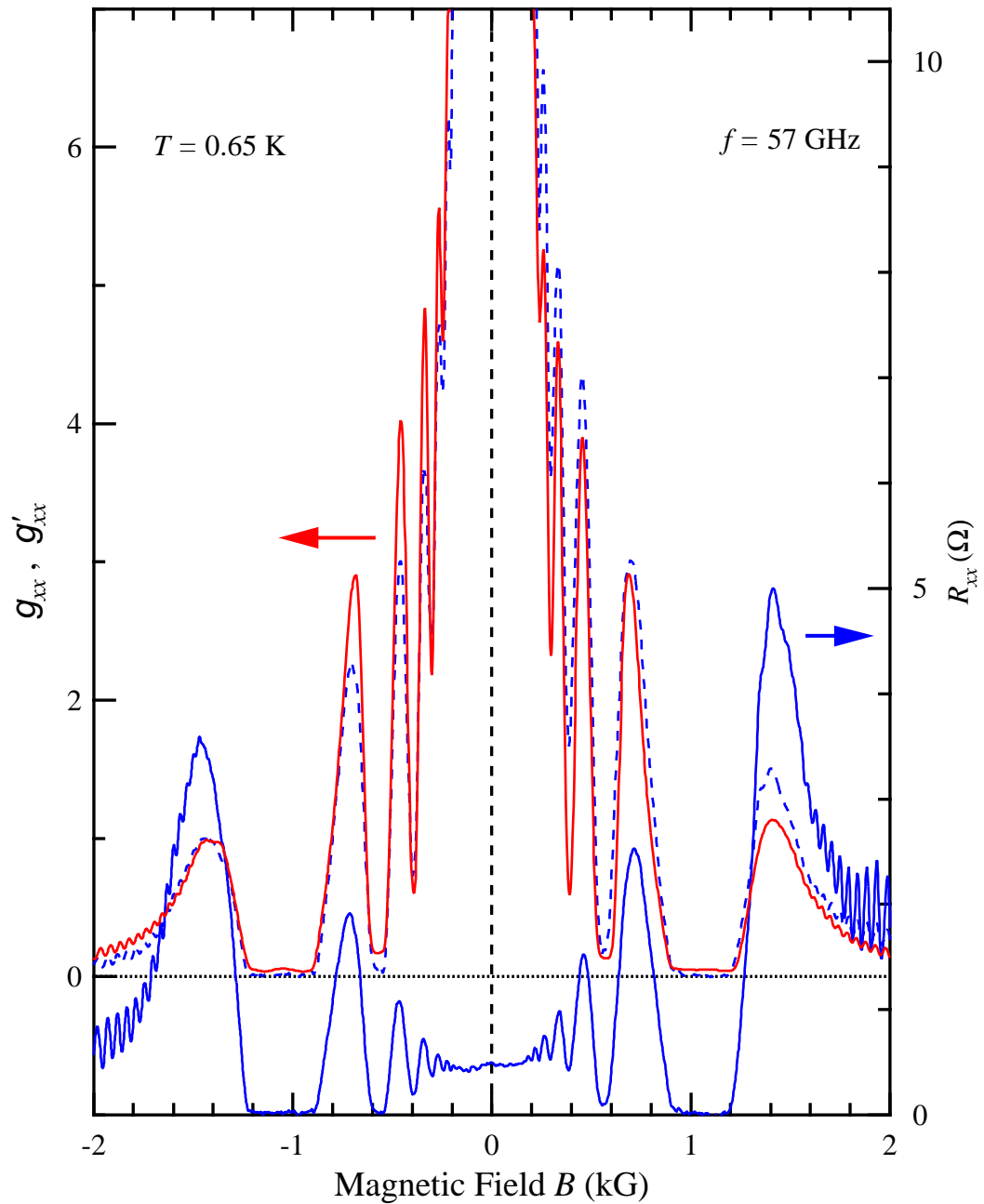
Figure 4.10. The measured g_{xx} (normalized conductance, as defined in the text) of a Corbino sample is shown together with g'_{xx} (dotted line) inverted via Eq. 4.2 from R_{xx} measured on a square sample. Excellent agreement between the measured g_{xx} and calculated g'_{xx} is found.

The signal was then averaged using a pair of sweeps with alternating bias polarity. Under the same experimental conditions the conductance traces measured in this way are nearly identical to those measured using a low-frequency lock-in technique (quasi-dc, shown in Fig. 4.5 and 4.6). The inset of Fig. 4.11 shows G_{xx} (dc) traces around the ZCS minimum taken with different bias voltages. Notice that the G_{xx} is shown on a logarithmic scale; similar to that found in quasi-dc measurements, a small residual conductance ($G_{xx} \lesssim 1.5 \times 10^{-5}$ S, at 1 mV) can be seen at low temperatures. On this scale the ZCS minimum exhibits a reproducible doublet shape.

Linear electrical transport is observed in ZCS in a large range of bias up to 10 mV in this sample. In Fig. 4.11 we present an G_{xx}–V curve measured on ZCS for a MW frequency $f = 57$ GHz, along with a G_{xx}–V curve at the first oscillation maximum for comparison. A linear I–V regime (constant G_{xx}) can be found for small bias, $V < 10$ mV, followed by a nonlinear regime, $V > 10$ mV, where a gradual increase (or decrease) of conductance at the oscillation minima (or maximum) is observed.

Before discussing the origin of the non-linear regime it is useful to estimate the electric field strength in the bulk of the 2DES. Note that the electric field, E_x, along the radius of the Corbino ring, depends on the radial position; in our samples the E_x on the inner perimeter is about 6 times of that on the outer perimeter. The top axis on Fig. 4.11 shows the estimated maximum E_x (i.e., on the inner perimeter).

Our data at large bias, $V > 10$ mV, can be interpreted as due to the electron heating effect in the presence of a bias E_x above 0.2 V/cm. Notice that, at further larger bias ($V > 100$ mV), the conductance curves at the minimum and maximum overlap one another which means the oscillations totally disappear. One of the possible mechanisms for such a heating effect is the Zener tunneling between Landau orbits at a low magnetic field, relevant to the ZCS regime. We have observed Zener tunneling effect [2] at a magnetic field ~ 1 kG where conductance of a 2DES resonates due to opening of new scattering channels. Such tunneling events take place at a characteristic electric field of ~ 1 V/cm. Recall also that this
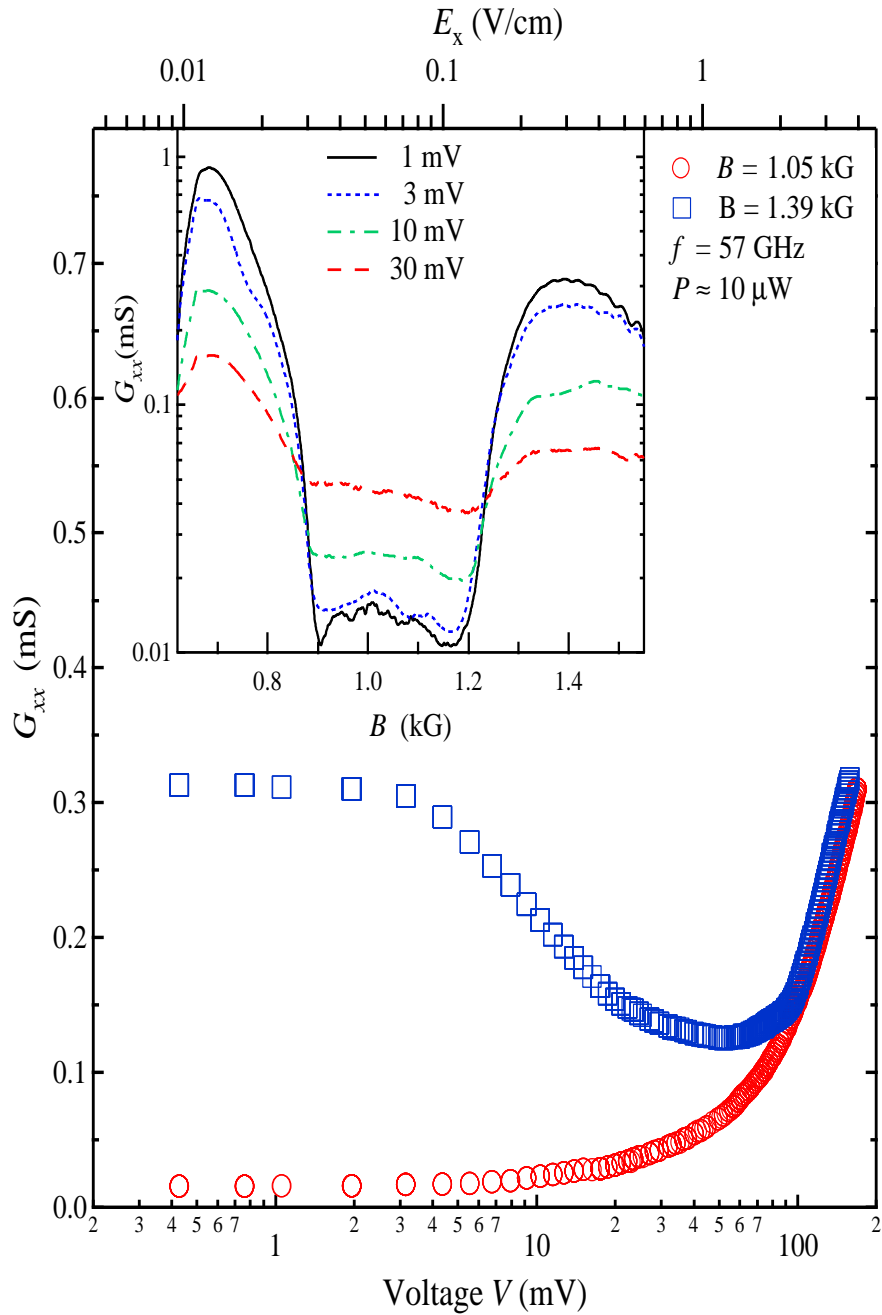
Figure 4.11. The conductance, G_{xx}, deduced from I–V curves measured at the first minimum (circle points) and the first maximum (square points), respectively, are shown as a function of applied bias voltage V. Microwave power is approximately 10 μW. Top axis shows an estimate for maximum (close to the inner perimeter of the Corbino sample) electric field, E_x. The insert shows conductance traces at selected bias voltages.

has been discussed in Chapter 3. It appears possible that Zener tunneling between Landau orbits occurs in some part of the Corbino sample giving rise to the nonlinear conductance. Variable-range hopping conductance can also be promoted by an increasing E_x [51].

4.3.5 Conductance oscillations at different MW frequencies

In addition, we have measured the conductance at different MW frequencies (from 25.5 GHz to 130 GHz) but at roughly the same MW power $P \approx 10~\mu$W (on the sample surface) and the same temperature $T \approx 0.65$ K. Selected conductance traces against $\varepsilon = \omega/\omega_c$ are shown in Fig. 4.12. Strong oscillations as well as the ZCS are observed at all MW frequencies. The period and the phase of the oscillations seen here are consistent with those observed in ZRS [4, 52]. We also notice a trend in which the strength of the oscillations, as measured by the peak height, is decreasing with increasing frequency. Such an observation can be partially accounted for by the number of photons incident on the 2DES. Since the MW power is roughly the same, the number of photons is inversely proportional to the MW frequency, leading to a diminishing of the oscillations at higher f. For $f < 40$ GHz, an additional maximum at $\varepsilon \approx 1/2$ is observed; an example can be seen on the $f = 30$ GHz trace. Such additional peaks have been previously seen in the ZRS experiments [4] and could be attributed to multiple-photon processes [52].

4.3.6 Summary of the conductance measurements

In conclusion, we have observed a MW-induced zero-conductance state in a high-mobility 2DES of Corbino geometry. While the effect is driven by an ac microwave field, the dc conductivity and the resistivity are found to be invertible using the standard dc transport tensor relation. Combining both the ZCS (in a Corbino sample) and ZRS (in a Hall bar sample), we present evidence for a new dissipationless 2D electronic transport effect induced by microwaves. The electrical transport in the ZCS regime is ohmic in the small bias limit; at larger bias, the
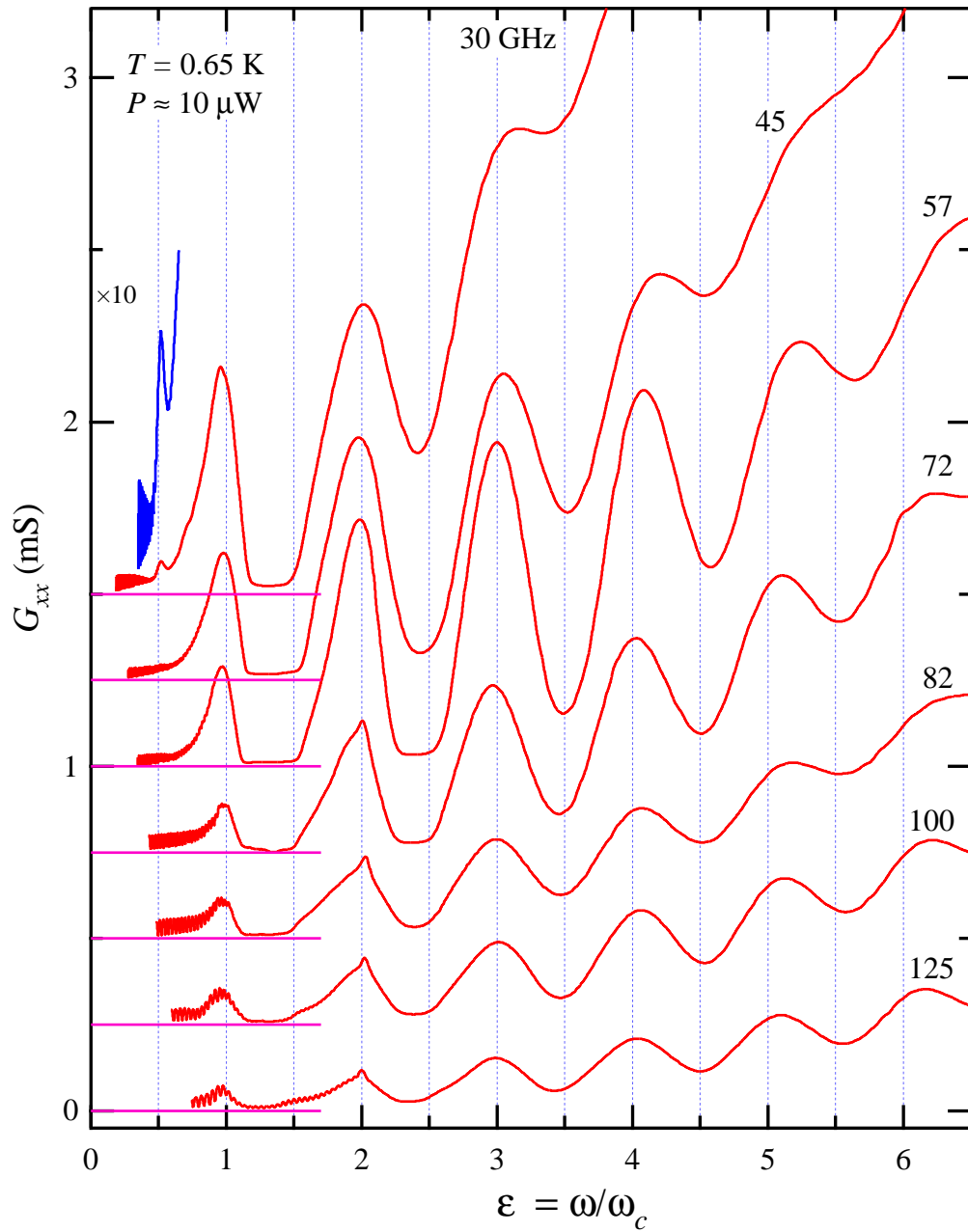
Figure 4.12. The conductance oscillations of the Corbino sample for selected MW frequencies with roughly the same $P \approx 10~\mu$W and $T \approx 0.65$ K (for clarity, traces are vertically shifted in steps of 0.25 mS), plotted against $\varepsilon = \omega/\omega_c$ with $m^* = 0.068\,m_e$. For all frequencies, strong oscillations as well as the ZCS are observed.

transport is affected by electron heating. Such observations indicate that the ZCS is remarkably robust, a fact which is consistent with an unusually large energy scale associated with such states. How these macroscopic properties relate to the theoretical models, especially to the proposed microscopic inhomogeneous phases [41, 42, 43, 45], is a subject for further experimental and theoretical work.

4.4   Survey for theoretical explanations

The observation of the MW-induced ZRS has stimulated considerable current theoretical interest in the research community [39, 40, 41, 42, 43, 44, 45, 46]. The origin of the ZRS is proposed to be either the self-organization of sliding charge density waves [39], or a instability caused by a absolute negative conductivity (ANC) [41, 42] at the MW-induced oscillation minima, or a quantum interference effect in a 2DES [53].

The instability of 2DES with a negative conductivity and its connection to the ZRS is shown by Andreev *et al* [41] and further justified by Vavilov and Aleiner [54]. They have shown that, independent of the microscopic details, a state with negative conductivity is absolutely unstable; the consequence of this instability is that the system rearranges itself to form current domains (for a system with Hall bar geometry) with a local current $j_x = j_0$ and local electric field $E_x = 0$, giving rise to the macroscopically observed ZRS. Based on this scenario, understanding the ZRS becomes the task of addressing: a) the origin of the MW-induced oscillations, and b) the occurrence of ANC at the oscillation minima.

Since there are experimental results that favor the existence of ANC at the ZRS regime [55], in the following paragraphs I will only present more details for the origin of the MW-induced oscillations and the subsequent ANC at the minima.

To illustrate how the MW can induce oscillatory dc conductance, a simple picture adapted from Ref. [40] is shown in Fig. 4.13. In this picture, an electron absorbs energy $\hbar\omega$ from a photon and is promoted to a *virtual* state somewhere among the stationary Landau levels which are spatially tilted by the probe dc voltage. The excited electron can be scattered forward or backward along the
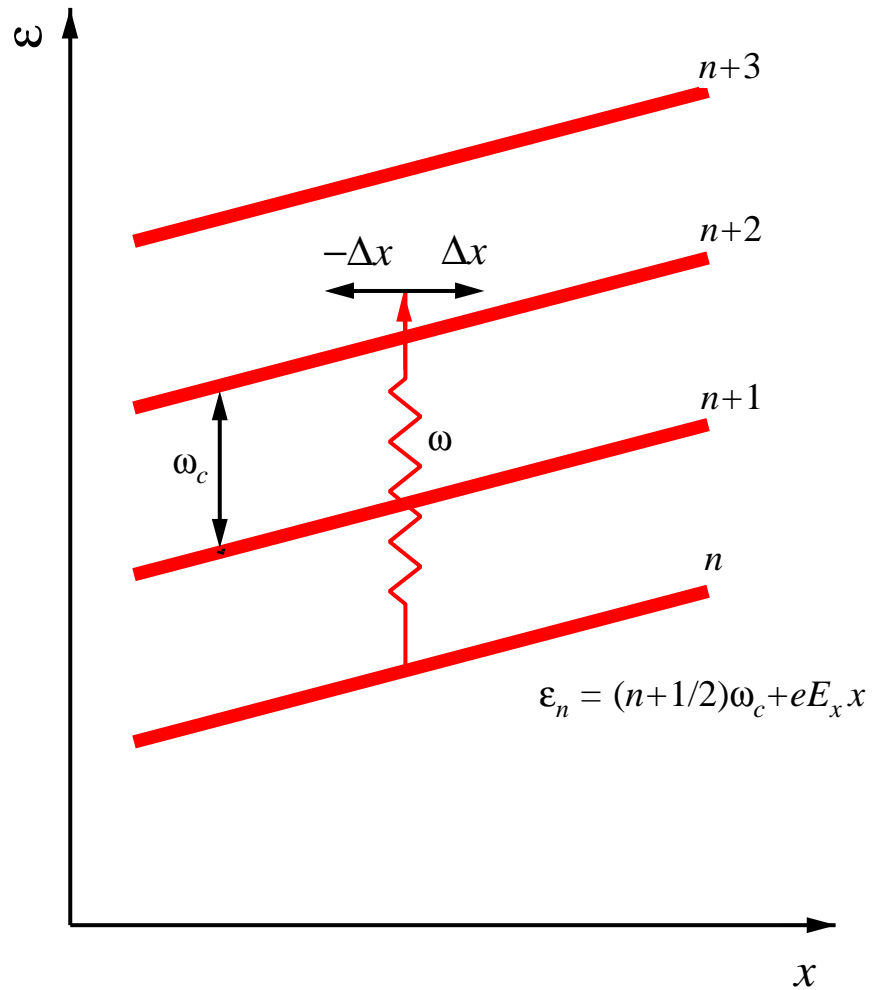
Figure 4.13. A simple picture for the MW-induced-photoconductivity resonance. The Landau levels are tilted by the applied dc bias electric field E_x. Electrons absorb photons and are excited by energy ω. Photoexcited electrons are scattered by disorder and kicked to the right or to the left by a distance Δx. If the final density of states to the left exceeds that to the right, dc current is enhanced. If vice versa, dc current is diminished. [Adapted from Ref. [40].]

dc voltage by impurities, causing a negative or positive dc current. The total current depends on the rate difference between the forward scattering and backward scattering, which is proportional to the difference in the density of states of the final states. Consequently, it is proportional to the derivative of the density of states at the specific energy of the virtual electron. Since the density of states is periodic in Landau level spacing $\hbar\omega_c$, the current induced should depend only on the position of the excited electron relative to the nearest Landau level. it is clear that this relative position is an oscillatory function controlled by the ratio $\epsilon = \omega/\omega_c$, and so does the total induced dc current. This explains the oscillatory dc conductance observed. The induced conductance is negative at the oscillation minima. With sufficient MW intensity, the oscillation can be so strong that at a minimum the induced conductance can overcome the background conductance and cause a net negative conductance or absolute negative conductance (ANC).

One serious question raised in the simple picture of Fig. 4.13 is that how the electrons can transit between Landau levels with index difference $\Delta n \geq 2$ since there is no nonzero matrix elements between these states through the dipole coupling of electrons to the microwave. In a perturbative picture, the answer is that the electrons are promoted by MW to a *virtual* state through high-order perturbation involving many Landau levels. In a non-perturbative picture, the microwave field should be directly included into the Hamiltonian and hence both the energy levels and wavefunctions are time-dependent [43, 56, 57]. According to an exact solution [57] to the Hamiltonian where the MW field is taken as an uniform ac electric field, an electron initially at Landau level $|n\rangle$ without MW can be mapped into a set of stationary energy levels with energy $\epsilon_n \pm m\hbar\omega$ after the MW is introduced, where ϵ_n is the Landau level energy without MW, m is an integer and ω is the MW frequency. Hence, the electron transition shown in Fig. 4.13 can be understood as a mapping of a time-dependent electron level (which is corresponding to ϵ_n if without MW) to the stationary level $\epsilon_n + \hbar\omega$.

As for the mechanism of ANC, it has been shown that, in addition to the impurities, the acoustic phonon scattering [58, 59] or a small change in the electron mass due to the MW irradiation [44] can also produce the ANC.

CHAPTER 5

POSSIBLE APPLICATION OF THE NEW OSCILLATIONS TO THE STUDY OF COMPOSITE FERMIONS

5.1 Quantum Hall effect

The quantum Hall effect(QHE) [60, 61] consists of the integer quantum Hall effect (IQHE) discovered by von Klitzing *et al.* [62] and the fractional quantum effect (FQHE) discovered by Tsui *et al.* [63], which is observed in very strong magnetic field (typically $B \sim 10$ T) at low temperatures ($T < 4$ K). In magneto transport, the QHE exhibits precise plateau in Hall resistivity at the vicinity of an integral or fractional filling factor ν

$$\rho_{xy} = \frac{\hbar}{\nu e^2},$$ (5.1)

where ν is an integer or simple rational fraction. Corresponding to a Hall plateau the diagonal resistivity (σ_{xx}) is almost vanishing at sufficiently low temperatures. A nice overview of experimental transport traces on IQHE and FQHE is presented in Figure 5.1.

The IQHE can be understood in a single electron picture with localization by impurities in a strong magnetic field. It is established that, at high magnetic field, most of the electron states are localized except those at the center of Landau levels. The regions of localized states are called *mobility gaps* and their boundaries with the extended states are *mobility edges*. In the mobility gap, the electrons have no contributions to the conductivity. At an integer filling factor, the Fermi level is at the center of a mobility gap (in the middle of two adjacent Landau levels). So if the filling factor is varied at the vicinity of an integer, the Hall conductivity will keep
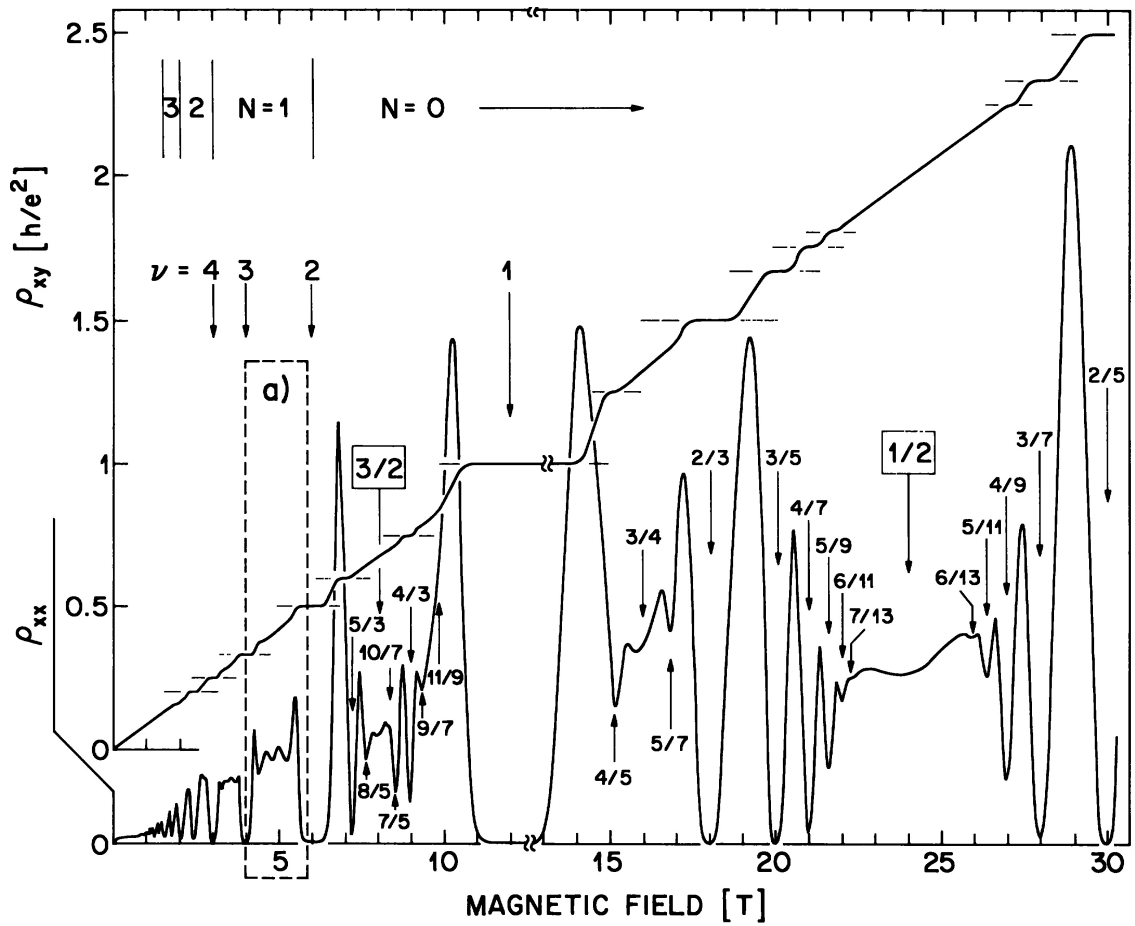
Figure 5.1. Diagonal resistivity and Hall resistivity Traces showing integer and fractional quantum Hall effect. [adapted from Ref. [64].]

constant and so does the vanishing diagonal conductivity. Transition from plateau to plateau happens when the Fermi level is swept across a mobility edge.

However, the FQHE is mainly due to the many-body interactions between electrons, and the 2DES has proven to be a unique playground for the study of many-body physics in the FQHE regime. Many significant accomplishments have been brought about by the study of FQHE and have contributed tremendously to the advance in condensed-matter physics. Theoretically, the FQHE has been addressed by various approaches and understood by different point of view. One of the sound theories is based on a new kind of quasiparticle called a *composite fermion*, possibly providing a unified view of the FQHE [65]. This will be discussed in next section.

5.2   Composite fermions

The composite fermion (CF) was proposed by J. K. Jain [66] to account for the fractional quantum Hall effect series at

$$\nu = \frac{p}{2mp \pm 1}. \tag{5.2}$$

Jain pointed out that there is a mapping between this series of FQHE to the IQHE. By attaching an even number ($2m$) of zeros of the many-body wavefunction to each electron, the system can be regarded as a collection of weakly interacted *composite fermions*. A composite fermion can be envisaged as an electron carrying an even number ($2m$) flux quanta ($\phi_0 = h/e$) and experiences and *effective* magnetic field

$$B^* = B - 2m\phi_0 n_e, \tag{5.3}$$

where the electron density n_e is also the density of the composite fermions. The composite fermions also form Landau levels in this effective magnetic field, with a cyclotron frequency and filling factor given by

$$\omega_c^* = \frac{e|B^*|}{m_{CF}}, \tag{5.4}$$

$$\nu^* = \frac{n_e h}{e|B^*|}. \tag{5.5}$$

where m_{CF} is the effective mass of a composite fermion. The filling factor for electrons $\nu = n_e h/eB$ can then be expressed by ν^* as

$$\nu = \frac{\nu^*}{2m\nu^* \pm 1}, \tag{5.6}$$

which is exactly the form of Eq. 5.2. Thus the FQHE of electrons at filling factor $\nu = p/(2mp \pm 1)$ can be mapped onto the IQHE of composite fermions at filling factor $\nu^* = p$, and the FQHE and IQHE are unified in this way.

The composite fermion picture is supported by a Chern-Simon field theory and also by various experimental observations. In particular, the composite fermion model predicts a well-defined Fermi surface of composite fermions at $B^* = 0$ ($\nu = 1/2m$), thus the behavior of the composite fermions around $\nu = 1/2m$ at high B can be mapped to those of the electrons at low B. These predictions are verified by various experiment techniques such as surface acoustic wave attenuation, geometric resonance, magnetic focusing, and SdH analysis. To date, it is widely believed that the composite fermion model contains most of the essence of the FQHE physics and it is a very good starting point for addressing the remarkably rich and complex properties of a quantum Hall system.

5.3 Search for the new magneto-oscillations of composite fermions

Since the discoveries of the new magneto resonances (see Chapters 2, 3, 4 of this thesis), we have attempted to search for these new effects around $\nu = 1/2$ within the context of the analogy between the composite femions and the electrons. Although experimentally it is proven to be extremely challenging, conceptually we believe such effects should be there and it is worthwhile to pursue along this direction. In following, some thoughts are presented for the work along this line.

The CF-acoustic phonon scattering at exact $\nu = 1/2$ have been experimentally studied [67, 68, 69] and it is found to be consistent with the CF theory. If the magneto-acoustic-phonon resonance (MAPR) is observable for CFs, the effective

mass of a composite fermion (m_{CF}) could be *directly* measured. This is of great significance since the m_{CF} possesses important information on the electron-electron interactions but so far is measured only *indirectly* and wide discrepancies exist. The regular resistance measurement may not be sensitive enough to observe MAPR because the measurement has to be performed at low temperature (at least below 1K, otherwise the the CFs are not stably formed) where the acoustic phonons with momentum $2k_F$ (energy > 5 K) are not populated. More sensitive methods such as thermopower measurement may be more suitable to the study of MAPR for CFs.

The magneto-zener-tunneling resonance (MZTR), if observed for CFs, not only can address the effective mass m_{CF}, but also can explore short-range interactions presented to CFs. In the Chern-Simons field theory of CFs, the electric field seen by CFs is also an effective electric field which is the physical electric field (measured by a voltmeter, equal to the Hall field of electrons) plus a Chern-Simons gauge electric field associated with the CFs. This effective electric field is equal to a Hall field at the effective magnetic field. However, so far all the theories are on the vanishing electric field limit, how a finite electric filed affects the energy spectrum of CFs has not been explicitly treated. Of course we can assume it is the effective electric field that enters the energy spectrum according to the mapping to electrons. However, this needs to be experimentally addressed, possibly by the MZTR. In our experimental survey, the difficulties arose from the large physical electric field (Hall field) induced by a relatively large dc current at $\nu = 1/2$ where the B is large. The electric field can easily disturb the 2DES such as causing large density inhomogeneity or even quenching the electron density, so that a large current sufficient to render a resonance can not be passed through the 2DES without deteriorating its quality. We think this is mainly a material issue, and can be improved in the future.

Moreover, the electrodynamical response of CFs is of great interest to study. The microwaves, in principle, would not destroy the CFs [57] because of the Kohn theorem [70] which states that in system with translation symmetry the relative motion of the particles is not affected by photons. However, also because of

the Kohn theorem, the CFs may hardly respond to a microwave, a fundamental reason which makes the task of resonating the CFs with MW quite non-trivial. Some modifications to the sample, for example a potential modulation, has to be introduced to break the translation symmetry (but not severely reduce the mobility) in order to promote the MW response.

REFERENCES

[1] M. A. Zudov, I. V. Ponomarev, A. L. Efros, R. R. Du, J. A. Simmons, and J. L. Reno, Phys. Rev. Lett. **86**, 3614 (2001).

[2] C. L. Yang, J. Zhang, R. R. Du, J.A. Simmons, and J. L. Reno, Phys. Rev. Lett., **89**, 076801 (2002).

[3] M. A. Zudov, R. R. Du, J. A. Simmons, and J. L. Reno, Phys. Rev. B **64**, 201311(R) (2001).

[4] M. A. Zudov, R. R. Du, L. N. Pfeiffer, K. W. West, Phys. Rev. Lett. **90**, 046807 (2003).

[5] R. G. Mani, J. H. Smet, K. von Klitzing, V. Narayanamurti, W. B. Johnson, and V. Umansky, Nature (London) **420**, 646 (2002).

[6] H. L. Stormer, Rev. Mod. Phys. **71**, 875 (1999).

[7] A. H. Kahn and H. P. Frederikse, in *Solid State Physics*, edited by F. Seitz and D. Turnbull (Academic, New York, 1959), Vol **9**, P. 257.

[8] R. Kubo, H. Hasegawa, and N. Hashitsume, Phys. Rev. Lett. **1**, 279 (1958).

[9] P. N. Argyres and L. M. Roth, J. Phys. Chem. Solids **12**, 89 (1959).

[10] E. N. Adams and T. D. Holstein, J. Phys. Chem. Solids **10**, 254 (1959).

[11] S. Titeica, Ann. Phys. (Leipzig) **22**, 129 (1935).

[12] D. Calecki, C. Lewiner, and P. Nozieres, J. Phys. (Paris) **38**, 169 (1977).

[13] L. M. Roth and P. N. Argyres, in *Semiconductors and Semimetals*, edited by R. K. Willardson and A. C. Beer (Academic, Now York, 1966), Vol. **1**, p. 159.

[14] P. N. Argyres, Phys. Rev. **117**, 315 (1960).

[15] E. Bangert, Z. Phys. **215**, 177 (1968).

[16] For a review, D. G. Seiler and A. E. Stephens, Chapter 18 in *Landau Level Spectroscopy*, edited by G. Landwehr and E. I. Rashba (Elsevier Science Publishers, North-Holland, 1991); ibid, J. Hajdu, chapter 17.

[17] For a review, R. J. Nicholas, chapter 13, in *Landau Level Spectroscopy*, edited by G. Landwehr and E. I. Rashba (Elsevier Science Publishers, North-Holland, 1991); ibid Yu. A. Firsov, V. L. Gurevich and R. V. Parfeniev, chapter 20.

[18] R. R. Gerhardts, D. Weiss, and K. v. Klitzing, Phys. Rev. Lett. **62**, 1173 (1989).

[19] R. W. Winkler, J. P. Kotthaus, and K. Ploog, Phys. Rev. Lett. **62**, 1177 (1989).

[20] C. L. Yang, M. A. Zudov, T. A. Knuuttila, R. R. Du, L. N. Pfeiffer, K. W. West, Phys. Rev. Lett. **91**, 096803 (2003).

[21] D. C. Tsui, Th. Englert, A. Y. Cho, and A. C. Gossard, Phys. Rev. Lett. **44**, 341 (1980).

[22] Th. Englert, D. C. Tsui, J. C. Portal, J. Beerens, and A. C. Gossard, Solid State Commun. **44**, 1301 (1982).

[23] G. Kido, N. Miura, H. Ohno, and H. Sakaki, J. Phys. Soc. Japan **51**, 2168 (1982).

[24] M. A. Brummell, R. J. Nicholas, J. C. Portal, K. Y. Cheng, and A. Y. Cho, J. Phys. C **16**, L579 (1983).

[25] D. R. Leadley, M. A. Brummell, R. J. Nicholas, J. J. Harris, and C. T. Foxon, Solid State Electron. **31**, 781 (1988).

[26] C. L. Yang, M. A. Zudov, J. Zhang, R. R. Du, J. A. Simmons, and J. L. Reno, Physica E **12**, 443 (2002).

[27] I. V. Ponomarev and A. L. Efros, Phys. Rev. B **63**, 165305 (2001).

[28] Later it is shown that the acoustic phonons involoved in 2D resonance transport are not necessary strictly 2D. In principle, 3D phonons with small q_z can also contribute to the 2D resonance transport because 3D Phonons with large q_z are largely suppressed at low temperature; however, in this context these 3D phonons can also be regarded as having 2D nature. For details, see Jian Zhang, S. K. Lyo, R. R. Du, J. A. Simmons, and J. L. Reno, Phys. Rev. Lett. 92, 156802 (2004).

[29] D. C. Tsui, G. J. Dolan, and A. C. Gossard, Bull. Am. Phys. Soc. **28**, 365 (1983).

[30] The resonance condition is Eq. (3.13). From Fourier analysis point of view, it gives an oscillatory resistivity $\rho_{xx} \propto \cos(2\pi l)$, where $l \propto J_{dc}/B$. Accordingly, the voltage $V \propto \rho_{xx} J_{dc} \propto J_{dc} \cos(2\pi l)$ and $r_{xx} \equiv \partial V/\partial I \propto \partial V/\partial J_{dc}$. It is easy to show that r_{xx} has a phase shift $\sim 90°$ with respect to ρ_{xx}, which can be largely restored by $\partial r_{xx}/\partial |B|$.

[31] C. Chaubet, A. Raymond, and D. Dur, Phys. Rev. B **52**, 11178 (1995).

[32] M. A. Zudov, I. V. Ponomarev, A. L. Efros, R. R. Du, J. A. Simmons, and J. L. Reno, Phys. Rev. Lett. **86**, 3614 (2001).

[33] H. L. Stormer, Surf. Sci. **132**, 519 (1983).

[34] T. Ando, J. Phys. Soc. Jpn. **51**, 3900 (1982).

[35] T. Saku, Y. Horikoshi and Y. Tokura, Jpn. J. Appl. Phys. **35**, 34 (1996).

[36] V. Umansky, R. de-Picciotto, and M. Heiblum, Appl. Phys. Lett. **71**, 683 (1997).

[37] A. D. Mirlin *et al.*, Phys. Rev. Lett. **87**, 126805 (2001).

[38] P. D. Ye, L. W. Engel, D. C. Tsui, J. A. Simmons, J. R. Wendt, G. A. Vawter, and J. L. Reno, Appl. Phys. Lett. **79**, 2193 (2001).

[39] J. C. Phillips, cond-mat/0212416.

[40] A. C. Durst, S. Sachdev, N. Read, and S. M. Girvin, Phys. Rev. Lett. **91**, 086803 (2003).

[41] A. V. Andreev, I. L. Aleiner, and A. J. Millis, Phys. Rev. Lett. **91**, 056803 (2003).

[42] P. W. Anderson and W. F. Brinkman, cond-mat/0302129.

[43] J. Shi and X. C. Xie, Phys. Rev. Lett. **91**, 086801 (2003).

[44] A. A. Koulakov and M. E. Raikh, Phys. Rev. **B** 68, 115324 (2003).

[45] F. S. Bergeret, B. Huckestein, and A. F. Volkov, Phys. Rev. B **67**, 241303(R) (2003).

[46] S. A. Mikhailov, cond-mat/0303130.

[47] M. A. Zudov, R. R. Du, J. A. Simmons, and J. L. Reno, cond-mat/9711149; M. A. Zudov, Ph.D. Thesis, University of Utah (1999).

[48] R. R. Du, M. A. Zudov, C. L. Yang, L. N. Pfeiffer, and K. W. West, Physica E **22**, 7 (2004).

[49] See, e.g., D. C. Tsui, H. L. Stormer, and A. C. Gossard, Phys. Rev. B **25**, 1405 (1982).

[50] See, e.g., S. Das Sarma and D. Z. Liu, Phys. Rev. B **48**, 9166 (1993).

[51] See, e.g., D. G. Polyakov and B. I. Shklovskii, Phys. Rev. Lett. **70**, 3796 (1993); Phys. Rev. B **48**, 11167 (1993).

[52] M. A. Zudov, Phys. Rev. B **69**, 041304 (2004).

[53] D. H. Lee and J. M. Leinaas, Phys. Rev. B **69**, 115336 (2004).

[54] M. G. Vavilov and I. L. Aleiner, Phys. Rev. B **69**, 035303 (2004).

[55] M. A. Zudov, C. L. Yang, R. R. Du, L. N. Pfeiffer, K. W. West, unpublished.

[56] X. L. Lei and S. Y. Liu, Phys. Rev. Lett. **91**, 226805 (2003).

[57] K. Park, Phys. Rev. B **69**, 201301 (2004).

[58] V. Ryzhii and V. Vyurkov, Phys. Rev. B **68**, 165406 (2003).

[59] V. Ryzhii, Phys. Rev. B **68**, 193402 (2003).

[60] For a review, see *The Quantum Hall Effect*, edited by R. E. Prange and S. M. Girvin (Springer-Verlag, New York, 1990).

[61] *Perspectives in Quantum Hall Effect*, edited by S. Das Sarma and A. Pinczuk (Wiley and Sons, New York, 1997).

[62] K. von Klitzing, G. Dorda and M. Pepper, Phys. Rev. Lett. **45**, 494 (1980).

[63] D. C. Tsui, H. L. Stormer, and A. C. Gossard, Phys. Rev. Lett. **48**, 1559 (1982).

[64] R. Willett, J. P. Eisenstein, H. L. Stormer, D. C. Tsui, A. C. Gossard, and J. H. English, Phys. Rev. Lett. **59**, 1776 (1987).

[65] For a review, see *Composite Fermions: a unified view of the quantum Hall regime*, edited by O. Heinonen (World Scientific, Singapore, 1998).

[66] J. K. Jain, Phys. Rev. Lett. **63**, 199 (1989).

[67] W. Kang, S. He, H. L. Stormer, L. N. Pfeiffer, K. W. Baldwin, and K. W. West, Phys. Rev. Lett. **71**, 3850 (1995).

[68] B. Tieke, U. Zeitler, R. Fletcher, S. A. J. Wiegers, A. K. Geim, J. C. Maan, and M. Henini, Phys. Rev. Lett. **76**, 3630 (1996).

[69] V. Bayot, E. Grivei, H. C. Manoharan, X. Ying, and M. Shayegan, Phys. Rev. B 52, R8621 (1995).

[70] W. Kohn, Phys. Rev. **123**, 1242 (1961).